## Proprotor Design Issues for High Speed Tiltrotors

Leo Dadone Technical Fellow, Aeromechanics

John Liu Senior Technical Specialist

Joseph Wilkerson Senior Staff Engineer Boeing Defense & Space Group Helicopter Division

and

C.W. Acree Aerospace Engineer NASA, Ames Research Center

CI

#### **ABSTRACT**

This paper presents key findings from an analytical investigation carried out to identify technologies critical to the feasibility of advanced rotorcraft proprotors. The focus was on high speed tiltrotors, exhibiting both high cruise propulsive efficiency and helicopter-like hover efficiency, providing a low-risk design capability for advanced rotorcraft by the year 2000.

It was concluded that 400 knot proprotors are feasible with existing aerodynamics and structure technology. Blade planform sweep would be needed for operation at and above 400 knots. Blade designs for operation below 380 knots should be possible without significant sweep. The results of the study also imply that thickness effects at the root are as much of a design issue as transonic effects at the tip. Hub configurations and interactional aerodynamic effects have a significant impact on the vibratory characteristics of high speed proprotors, and will require the use of carefully validated multi-disciplinary methods of analysis. Noise criteria will also have to be introduced as explicit design objectives in future tradeoff studies.

#### SYMBOLS

Α	rotor disc area, ft <sup>2</sup>
С	airfoil or blade chord, ft
Cd	sectional drag coefficient
	ented at the 50th Annual Forum of the American opter Society, Washington, DC, May 1994

$c_p$	rotor power coefficient
CT	rotor thrust coefficient
D	drag force, lb
El	flapwise, or chordwise blade stiffness
FM	rotor figure of merit, in hover
GJ	torsional stiffness
<i>i</i> p	propeller incidence angle, with respec

sectional lift coefficient

k<sub>MACH</sub> scaling factor, used in Figure 4

stream, degrees

L lift force, lb

M Mach number

M<sub>DD</sub> drag divergence Mach number

r (or x) spanwise position along blade, ft

Q torque, ft-lb

R rotor radius, ft

t maximum thickness of airfoil section, ft

T rotor or propeller thrust, lb

Up perpendicular component of wing / fuselage interference velocity at computation point on a blade, defined in the rotor disc coordinate system, ft/sec UR radial component of interference velocity Uт tangential component of interference velocity ٧i local induced velocity component, ft/sec local free-stream wind component, ft/sec Vo resultant velocity, used in Figure 5 V<sub>R</sub> Vт blade tip speed (ΩR), ft/sec ٧... remote wind or flight velocity, ft/sec α angle of attack, degrees 3 local twist angle, degrees propulsive efficiency η θ blade pitch angle, degrees θ75R collective pitch angle, referenced to the 0.75R blade station ٨ blade sweep angle (generally quarter-chord sweep), degrees rotor advance ratio, V/VT μ air density, slugs/ft3 ρ. σ<sub>T</sub>, σ rotor thrust-weighted solidity local flow angle, degrees Ψ blade azimuth angle, degrees Ω rotational velocity, rad/sec

#### BACKGROUND

The current and continuing interest in civil tiltrotor aircraft results from a combination of technology advances and the ever increasing congestion at airports serving large metropolitan areas. This congestion cannot be relieved by just building new airports because it has become very difficult to find suitable land within a practical distance from major urban centers. Tiltrotors, combining the takeoff and landing versatility of helicopters and the speed of fixed wing aircraft, hold an answer to growing high-speed inter-city transporta-

tion needs without the real estate investment of conventional airports. A recent civil tiltrotor missions and applications study sponsored by NASA/FAA<sup>1</sup> demonstrated conclusively that a market exists for a commercial passenger tiltrotor. At the same time, NASA-funded studies of advanced high-speed rotorcraft<sup>2</sup> concluded that an advanced tiltrotor (or tiltwing) in the 450 knot speed range is feasible for future civil and military missions.

Affordability is the key issue. Affordability means higher cruise speeds to reduce maintenance costs per trip, high reliability, and high availability, with the simplest design implementation. Our total experience with tiltrotors is encouraging, but relatively limited. The XV-15 was the pathfinder. The V-22 has demonstrated the practicality of the concept for highly demanding Marine and Navy missions. Now we need to design for the speed, efficiency and reliability required by the cost-driven civil market, for the smooth, quiet ride required by the passengers, and for the low noise required by the public.

High speed and high performance propellers have been demonstrated on fixed wing aircraft, but it is not clear to what extent the propeller experience is applicable to large diameter and low disc-loading proprotors with hover, axial flight and transition flight requirements. In order to quantify the key elements of the problem, NASA sponsored a study to look into some of the design features and limitations of large proprotors for high-speed tiltrotor applications3. This study, completed in August 1993, covered design, aerodynamics, noise and aeroelastics issues, but was not meant to yield fully optimized proprotor configurations. Its objective was to examine and quantify key trends and effects which will have to be better understood before optimal tiltrotor aircraft designs can be defined. The focus was to provide low-risk design capabilities for high speed civil tiltrotors by the year 2000.

This paper draws on the NASA study<sup>3</sup>, but it is limited to proprotor performance in hover and cruise, interactional aerodynamics, blade transonic effects and elastic deflection effects based on preliminary blade structural properties.

#### INTRODUCTION

Before discussing the details of how the design of high speed proprotors can be addressed, it would be useful to describe some of the key aerodynamic phenomena involved.

Flow Environment - The flow environment of a prop-rotor blade in high speed flight is illustrated in Flgure 1 for an assumed 400 knot flight speed with a 600 ft/sec rotational tip speed. The flight and rotational velocities are added vectorially to illustrate how the local relative wind direction changes between the root and the tip of the blade.

At the root, the local flow is nearly perpendicular to the disc plane because close to the center of rotation the tangential velocity component is very small compared to the flight velocity. The local Mach number close to the root is M=0.67, which provides quite a challenge since compressibility would dictate a relatively thin root airfoil section (t/c < 0.15), while structural requirements would call for thick sections (t/c > 0.2).

The twist of high-speed proprotor blades is almost entirely dictated by the cruise design point. Since the whole blade operates in a high Mach Number, high dynamic pressure flow field, it is imperative that each blade radial station be carefully aligned with the local flow. Small angles of attack along the entire span of the blade are dictated by the need to avoid high compressibility drag penalties. At high cruise speeds, the local Mach numbers arising from the combination of rotational and flight velocities do eventually exceed the drag divergence capabilities of the airfoils employed along the blades. Figure 1 also illustrates quite clearly the fact that at the root of the blades the lift is nearly parallel to the disc plane, so that very little of the lift contributes to the thrust, and most of it is in the torque direction (although with a very short moment arm). Only further outboard does the local lift vector contribute a more significant component to the rotor thrust.

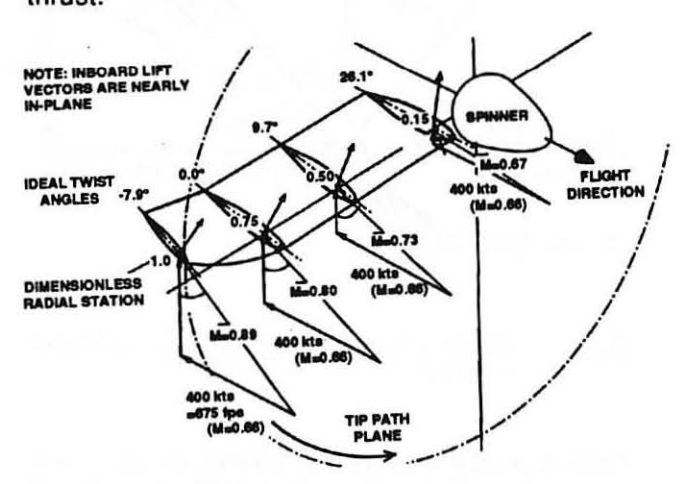


Figure 1 - Local flow environment over high speed proprotor blades

Tip sweep, of course, reduces the effective Mach number encountered by the blade's tip sections, but the introduction of tip sweep must take into account the fact that three-dimensional effects near the blade tip also reduce the effective local Mach number. The accurate assessment of compressibility effects close to the tip of high speed proprotor blades is a very difficult aerodynamic challenge.

Nominal, sweep-reduced and tip-effect reduced Mach number levels are illustrated in Figure 2. The LeNard approximation<sup>4</sup> of tip Mach number relief effects, applicable primarily to the drag, has been used quite successfully in conjunction with lifting-line models of rotor blades and has been introduced in all Boeing Helicopters rotor analysis codes. Other empirical corrections have been introduced in the codes to account for 3-D effects on the lift. As discussed in a later section, the modeling of tip flows has been investigated by rotor CFD methods. The relative placement of the airfoil drag divergence Mach number boundaries and of the local operating Mach number conditions, at 450 knots, are illustrated in Figure 3 for two modern airfoils (VR-12 and VR-15).

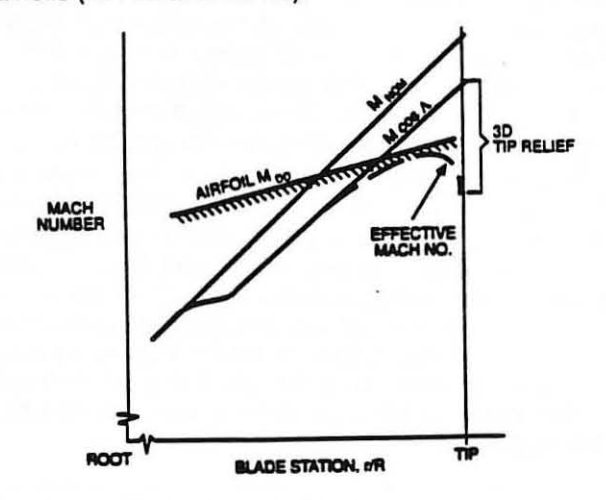


Figure 2 - Blade tip Mach Number environment

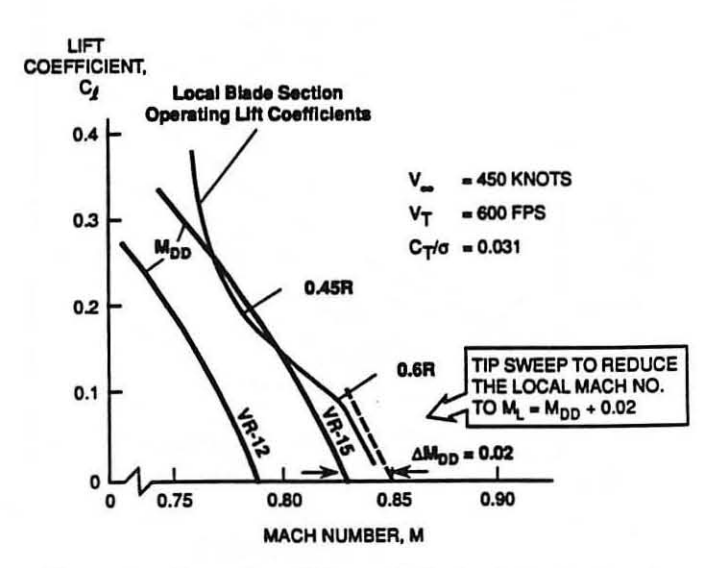


Figure 3 - Operational lift coefficient relative to the drag divergence boundary

<u>Power Consumption</u> - In cruise, the proprotor power consists of three components: propulsive or useful

power, profile power, and induced power loss. In axial flight, the rotor power coefficient can be expressed as

$$CP = k_{Mach}C_{Pprofile} + \mu C_T + C_T^2/2\mu$$

Figure 4 shows the power required to generate one pound of thrust over a range of cruise speeds computed for 25,000 ft standard-day atmospheric conditions. The magnitude of the different contributions to the total power is also shown. The propulsive, or "useful" component, μCT, is the largest contribution and it represents the power needed to produce the thrust required for a given forward speed. At high cruise speeds the axial induced velocity is low because of the low cruise thrust requirements and low disc loading (typically 10 to 20 percent of the hover disc loading). For instance, in the speed range between 300 and 400 knots, the average axial induced velocity is less than 2 ft/sec. Hence, the induced power, given by CT2/2µ, is small and becomes even smaller as the advance ratio increases. The profile power losses, given by kMachCpprofile, are due to blade drag and increase with speed due compressibility drag rise. kmach is the compressibility drag rise factor and is a function of blade section airfoil characteristics. Since the required propulsive power can be assumed to be fixed for a given cruise speed, and the induced power is small, it becomes obvious that the efficiency of high-speed proprotors can be improved primarily by minimizing profile power losses.

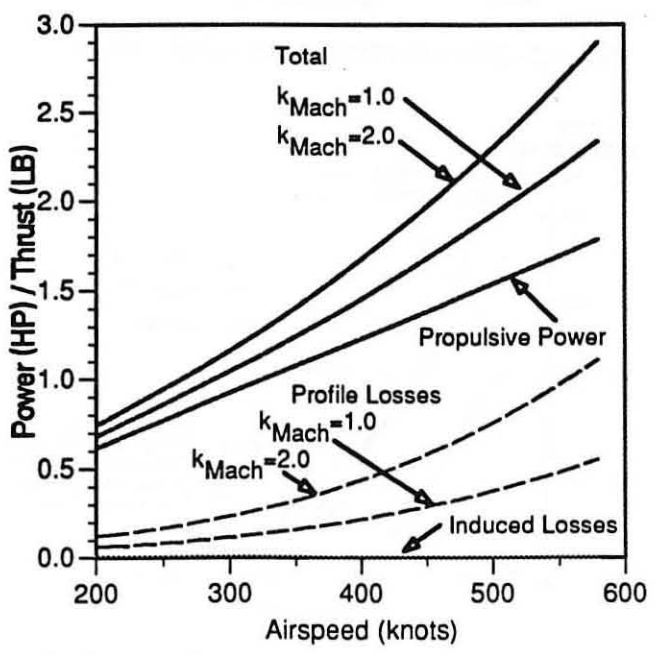


Figure 4 - Proprotor Propulsive Power Required, Profile Losses and Induced Losses

Figure 5 shows the velocity and force vectors for a typical blade section in axial flight. Although the in-

duced velocity is small compared to either the local rotational speed or the flight speed, its orientation relative to the resultant velocity causes an induced angle of attack which may not be negligible in the context of proprotor operation at high speeds. For instance, in 400 knot flight, the local induced angle along the blade, \alpha\_i, could be almost 1°. At high flight Mach numbers, a change in local angle of attack of that order of magnitude could severely penalize a proprotor in terms of compressibility drag rise. The total in-plane force that produces rotor torque is due to components of the sectional lift and drag forces. At 400 knot cruise speed, with 600 ft/sec tip speed, the inflow angle is close to 50° at the tip and 80° at the root. At these large inflow angles the lift contribution to the in-plane drag force (r·dL·sin φ) can be large. Therefore, when designing blades for high speed proprotors, it is important to distribute the blade loading so that the liftdependent torque and the torque due to blade drag are both minimized. As described later, while the optimum planforms for the hover and cruise flight conditions are very different, the final blade geometry must be compromised in favor of cruise.

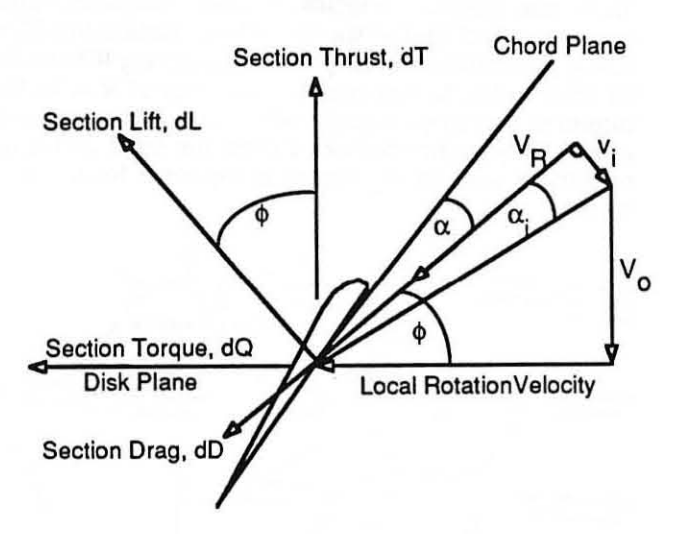


Figure 5 - Blade Section Velocity and Force Vector Diagram

From a profile drag point of view, an optimal high-speed rotor design requires airfoils with good Mach Number penetration to allow operation within the sections' drag divergence boundaries. Achieving this, it turns out, is not a simple task. The airfoil section requirements are driven by the outer 25% of the blade, operating beyond a Mach number of 0.8. The conventional helicopter rotor wisdom of designing for minimum induced power with the airfoil sections operating near maximum L/D simply does not apply here. One of the objectives of this study was to define the parameters necessary to achieve the "ideal" high speed performance, and to apply them, on a preliminary basis, to a practical rotor design.

<u>Aircraft Sizing Considerations</u> - Aircraft size and gross weight are sensitive to the design airspeed. A trend curve of tiltrotor gross weight versus design airspeed is shown in Figure 6 for a 25,000 ft cruise altitude. The configuration is an unswept wing with a horizontal tail. The wing thickness ratio was reduced to avoid drag divergence at the higher airspeeds, but the thin wing assumptions resulted in severe weight penalties to meet the wing stiffness requirements necessary to satisfy aerodynamic performance and whirl flutter stability constraints. Proprotor cruise efficiency also drops off beyond about 430 knots, adding to the growth in aircraft weight with design speed. The High-Speed Rotorcraft Study<sup>2</sup> solved the "thin wing" problems by employing canards and 30° of forward sweep on the wings, for a 450 knot design speed. However, as illustrated in Figure 6, for conventional tiltrotor configurations very substantial gross weight penalties can be expected for design speeds beyond 420 knots.

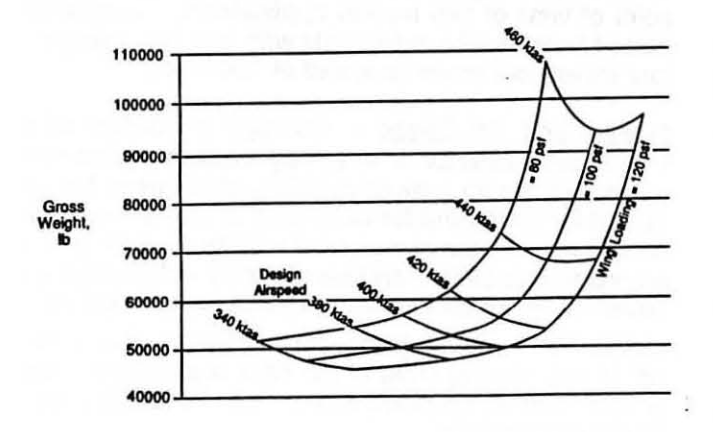


Figure 6 - Effect of design speed and wing loading on gross weight

However, many reasons remain to continue pursuing design studies at high airspeeds. High speed means shorter trip times, which should result in reduced operating costs per trip, giving the operator a greater profit margin, or allowing lower ticket prices. Productivity. defined as payload times airspeed divided by empty weight, is another way of quantifying speed benefits. Figure 7 clearly shows the increase in turboprop airspeed capability, leading to the 360 knot SAAB 2000 soon to be in service. The high speed turboprops have shown continued productivity improvements. The peak in the curve of productivity versus design airspeed has not yet been reached. Rather, the peak has been pushed to higher airspeeds through technology developments. This in itself is a compelling reason to continue studying and developing highspeed tiltrotor concepts. Having identified the technology needs, innovative designs and improved materials will turn concepts into capabilities.



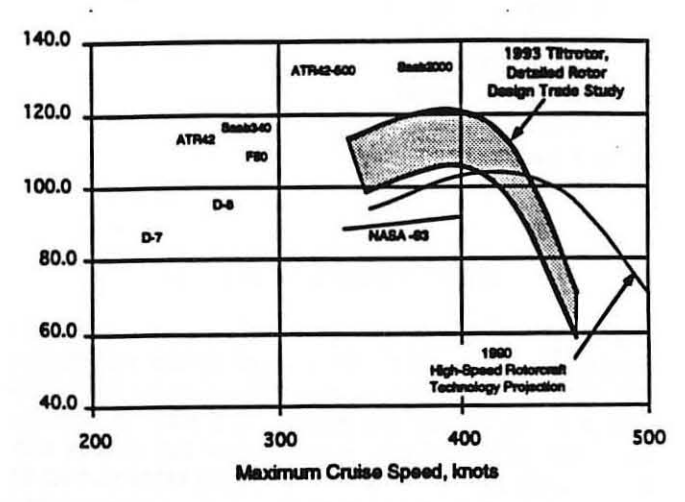


Figure 7- Effect of design speed on productivity

<u>Design Conditions</u> - The design conditions set forth at the start of the present study are summarized in **Table** I. The magnitude of the quantities called for are based on the results from NASA High-Speed Rotorcraft Study<sup>2</sup>, but tempered by the desire to avoid the technical challenge of designing swept wings.

### **DESIGN CONDITIONS** Baseline 40 passenger civil tiltrotor (CTR-22D, 4 abreast seating, circular fuselage) 400 KTAS at Cruise design speed: 25,000 ft altitude 20 psf at Hover disc loading: SL/ISA + 15°C Wing Loading: 100 psf Maximum L/D: 13.5 at 200 knots, SLS Cruise L/D: 10.2 at 400 knots, 25.000 ft Rotor cruise thrust: 2200 lb per rotor 37.1 ft Rotor diameter:

Table I - Summary of initial design conditions

The blade characteristics and rotor performance parameters to be defined are:

- o Number of blades
- o Rotor solidity
- Chord distribution
- o Airfoil distribution
- Twist distribution
- Tip sweep angle distribution
- o Blade tip speed
- o Hover CT/OT
- o Hover Figure of Merit
- o Cruise propulsive efficiency

#### ROTOR ANALYSIS CODES

The B-08<sup>5,6,7</sup> analysis was used almost exclusively during the definition of the design space and during the more detailed hover and cruise tradeoff investigation presented up to this point. For the hover calculations, the sectional characteristics of the airfoils employed over the root end of the blades were corrected on the basis of available test evidence<sup>8</sup> to approximate stall delay effects. B-08 results were compared with test data and also with the results of the CAMRAD-JA9 and the TECH-0110,11 codes. While restricted to the limitations of local momentum theory, B-08 results compared quite favorably with the CAMRAD-JA and TECH-01 comprehensive codes. CAMRAD-JA, TECH-01, VSAERO12 and the FPR13,14 codes were also used beyond the initial design investigation when the phenomena being addressed extended beyond the modeling capabilities of B-08. Specifically:

- o TECH-01 was employed to address the effect of elastic deflections of the blades, to introduce non-axisymmetric phenomena, to assess wing/fuselage interaction effects, and to provide a link between comprehensive rotor analysis and blade CFD calculations.
- o CAMRAD/JA. Since it is generally available in Government research centers and throughout industry, CAMRAD-JA was used to establish a basis for comparison with the B-08 and TECH-01 calculations. It was also used to estimate whirl flutter stability and conversion loads, which are documented in Reference 3, but are beyond the scope of the present paper.
- VSAERO was used to calculate wing and fuselage interference velocities, subsequently introduced into TECH-01.
- o FPR and a preliminary axial version of FPR were used to quantify three-dimensional, transonic tip relief effects. The FPR results were used to define empirical corrections for use with the lifting-line model of the blades used in TECH-01, as presented later in this pa-

per. Reference 3 describes the approach and computations in detail .

## INITIAL HOVER/CRUISE PERFORMANCE TRADE STUDY

As a first step, a trade analysis was conducted to determine general hover and cruise performance trends for unswept rotors, on the basis of the requirements and design constraints specified in **Table I**. The parameters reviewed in this initial assessment of design requirements included rotor solidity, tip speed, blade airfoils, twist, and chord distributions. On the basis of the results obtained, a baseline unswept blade was defined representing a starting point for further analysis, and leading to the development of designs better balanced in terms of compromises between hover and cruise.

Number of Blades - V-22 experience and previous civil tiltrotor design studies<sup>2</sup> have shown that, from the point of view of civil market applications, acceptable noise levels may be achievable with four blade proprotors limited to a hover tip speed of 700 ft/sec.

Solidity and Tip Speed - Although the design of a high-speed proprotor is driven by cruise performance objectives, thrust margin considerations must be included for hover and for maneuver at low-speed flight conditions. The thrust-weighted solidity of high-speed proprotor blades is therefore primarily determined by hover  $C_T/\sigma_T$  requirements. This imposes chordwise distribution constraints on the planform. Since the hover disk loading (T/A) of the rotor is specified, rotor solidity can be assumed to vary with hover tip speed by the relationship:

$$\sigma_{T} = C_{T_{hov}} / (C_{T}/\sigma_{T})_{hov}$$
$$= (T/A) / \{ \rho V_{T}^{2} (C_{T}/\sigma_{T})_{hov} \}$$

The hover  $C_T/\sigma_T$  of the rotor was selected on the basis of existing tiltrotor design trends. Figure 8 compares the disc loading and corresponding  $C_T/\sigma_T$  at the maximum gross weight hover conditions for the XV-15 (metal and Advanced Technology Blades 15) and the V-22 16, suggesting a preliminary design  $C_T/\sigma_T$  of 0.135 for the present study.

The hover tip speeds considered in the trend analysis were 650, 700, 750 fps. The cruise tip speed was chosen to be 100 fps less than in hover, resulting in corresponding cruise tip speeds of 550, 600, and 650 ft/sec. This was done to keep the cruise-to-hover RPM ratio in line with those of present generation

tiltrotors. In general, it is desirable to minimize the change in tip speed between hover and cruise in order to keep drive system weights to a minimum. As determined from the above relationship, the solidities corresponding to the three target tip speeds are therefore, 0.150, 0.134, and 0.117, respectively.

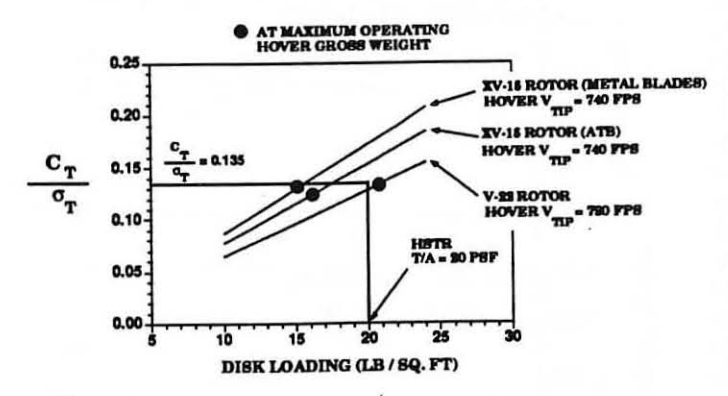


Figure 8 - Selection of design Hover  $C_{\perp}/\sigma_{\perp}$ 

<u>Chord Distribution</u> - For the initial trade study, only linearly tapered planforms were considered. For each solidity, taper ratios (tip chord / root chord) of 1:1, 2:3, and 1:3 were considered. The 3 solidities combined with the 3 taper ratios resulted in a total of 9 planform variations.

<u>Twist Distribution</u> - For the initial trade study, the twist distributions of the blades were assumed to be entirely defined by cruise inflow requirements. Separate twist distributions were therefore defined for each of the three tip speeds. Local twist adjustments were introduced later in the study.

<u>Airfoil Distribution</u> - The XN-18, VR-12 and VR-15 airfoils were used throughout the present study. Details of the airfoils, including contour information and sectional characteristics are presented in Reference 3.

The VR-12 and VR-15 airfoils (respectively (10.6% and 8% thick), were used without trailing-edge tabs for this application. They are suitable for high-speed cruise because of their high drag divergence Mach number characteristics (the zero-lift drag divergence Mach number for the VR-12 is MDDo = 0.803, and 0.835 for the VR-15). In hover they are relatively limited in lift because of their low camber level (specifically, at M = 0.6 their maximum lift capability is close to C<sub>Imax</sub> = 1.0, but the low-profile-drag range is limited to C<sub>1</sub> ≤ 0.6). Higher lift capabilities could be obtained by increasing camber, but this would penalize Mach number penetration and introduce higher sectional pitching moments. On helicopter rotor blades, the sectional pitching moments have a major effect on blade torsional deflections and control loads. Until the

design requirements for tiltrotor blades are better understood, the pitching moment constraints should not be significantly relaxed.

In the present study, an 18% thick root-end section was employed on the assumption that it may be structurally inappropriate to use thinner sections at the root. With the present blade radius of 18.55 ft, and a root chord between 3 and 4 feet, the 10.6% thick VR-12 section, applied at the root, would yield a root thickness of 3 to 5 inches. The same root chords, with an 18 percent thick airfoil section, would result in root thicknesses of 7 to 9 inches. While the XN-18 airfoil has high maximum lift capabilities at low Mach numbers, its drag divergence Mach number characteristics are relatively modest, with a zero-lift drag divergence value  $M_{DDO} = 0.715$ . This may be adequate for the 400 knot cruise speed application since, with a 600 ft/sec tip speed, the root-end Mach number of the resultant flow is close to 0.68. A section thicker than 18%, however, would probably operate beyond the drag divergence boundary, unless the root end of the blade could be swept (forward, as already done on some high performance propellers)

#### DESIGN CRUISE CONDITION 400 KNOTS AT 25,000 FT / STANDARD DAY

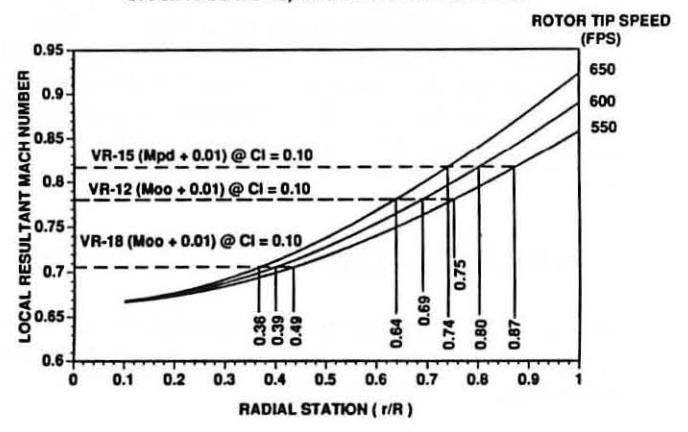


Figure 9 - Criteria for airfoil placement in cruise

The XN-18, VR-12 and VR-15 airfoils were distributed along the blades to minimize compressibility drag rise in cruise. Since the sectional drag divergence Mach number,  $M_{DD}$ , is a function of lift, which is not known apriori, the spanwise location of the airfoils was initially determined by matching the local resultant Mach number with  $(M_{DD}^+ + 0.01)$  at  $C_I^- = 0.10$ , a representative average lift coefficient for the thrust levels required in high speed cruise. Because of the small profile drag penalty involved, a Mach number margin  $\Delta M_{DD}^- = 0.01$  was added to allow a slight penetration beyond drag divergence. Figure 9 shows the Mach number environment along a blade for 400 knot cruise flight with tip speeds of 550, 600 and 650 ft/sec. The Mach

number level corresponding to  $(M_{DD} + 0.01)$  at  $C_{\parallel}$ =0.10 is shown for each of the airfoils. Since the Mach number increases with tip speed, the primary airfoil sections (VR-12 and VR-15) are placed further inboard as the tip speed increases.

Initial Performance Assessment - Nine blades were defined, representing three variations in taper ratio {1.0, 0.67, 0.33} and three levels of solidity {0.155, 0.134, 0.117). A solidity was determined for each of three hover/cruise tip speed combinations: 650/550, 700/600, and 750/650 ft/sec. A summary of the solidity and taper-ratio trade study is given in Figure 10. The bottom of Figure 11 shows the solidity values for the final hover and cruise tip speeds considered. The top plots, displaying Figure of Merit and cruise efficiency as a function of taper ratio, effectively summarize the feasible design space of a 400 knot proprotor as determined by preliminary groundrules and constraints. The most significant constraints are due to (a) the Mach number environment, set by ambient condition, tip speed and inflow, and (b) the blade loading.

These initial results show that, from among the nine rotors considered, the configuration with a 2/3 linear taper (thrust-weighted solidity,  $\sigma_{T}=0.134$ ), 700 ft/sec hover tip speed, and 600 ft/sec cruise tip speed, represents the best hover/cruise compromise. This configuration was, therefore, selected as the starting point for further improvement, to include the introduction of planform sweep. The hover Figure of Merit for this baseline rotor is 0.82. Its cruise propulsive efficiency is 77 percent.

#### INITIAL DESIGN OF A 400 KNOT SWEPT BLADE

The overall procedure for blade sweep design is summarized in Figure 11. The procedure consists of the following main elements:

- (a) Select a baseline unswept and untapered blade from the results of initial trade studies;
- (b) Refine the chord, twist and airfoil distributions to define the "best" blade loading at the design cruise condition:
- (c) Determine the drag divergence Mach number boundary corresponding to the lift distribution of the candidate "best" blade, and deduce the blade sweep distribution needed to alleviate drag rise due to compressibility.

<u>Initial Unswept Blade</u> - Based on the results of the preliminary trade study, an initial baseline unswept blade was selected as the starting point for swept blade

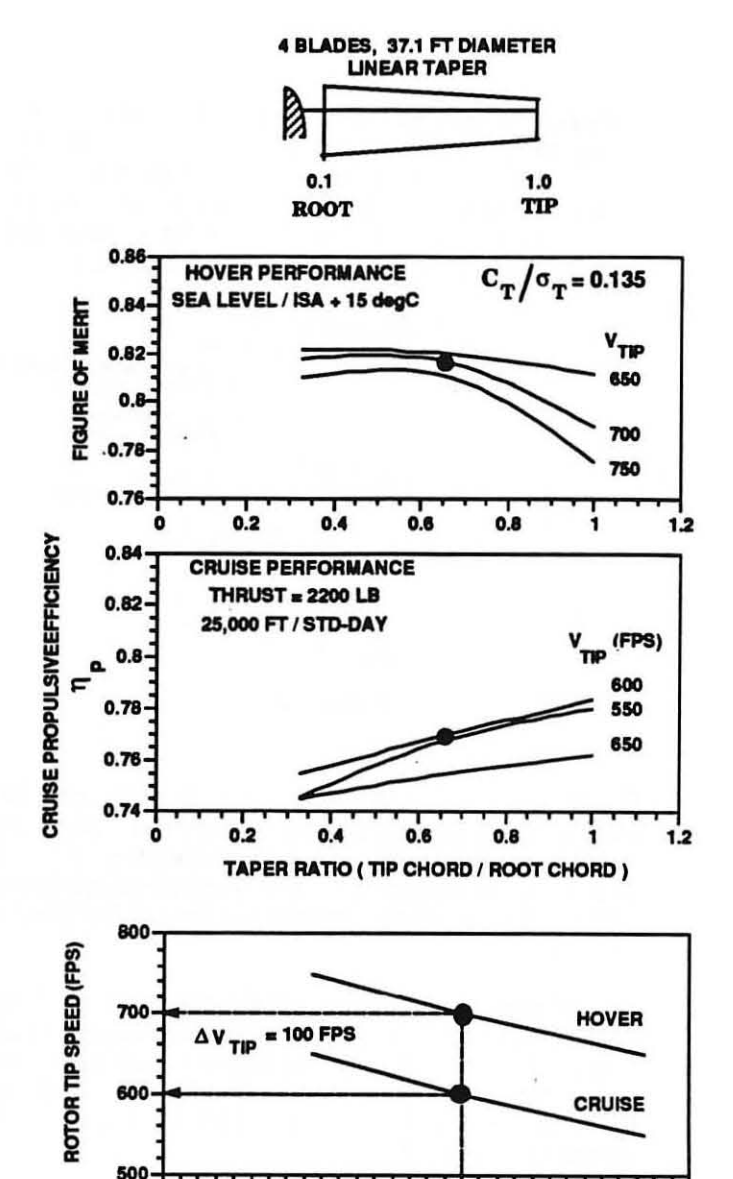


Figure 10 - Hover-Cruise feasible design space.

Results of initial solidity and taper ratio study

0.12

0.13

σт

0.14

0.15

0.16

0.1

0.11

design. This configuration had a thrust-weighted solidity of 0.134, a taper ratio of 2/3, and a hover and cruise tip speeds of 700 and 600 ft/sec, respectively. Its hover Figure of Merit was 0.82, and its cruise efficiency,  $\eta = 0.77$  at cruise design conditions. The objective was to examine realistic design alternatives which would improve upon the initial hover and cruise performance characteristics.

o Airfoil Distribution. It must be emphasized that the severity of compressibility effects on drag depends on the level of lift loading, which will later determine the amount of sweep required. The placement of the airfoils over the baseline unswept blade had to be progressively revised to yield a smooth lift distribution. Eliminating spanwise fluctuations in the blade loading I also eliminated unwanted excursions beyond the drag divergence boundary, M<sub>DD</sub>, and resulted in smoother definitions of blade sweep angles.

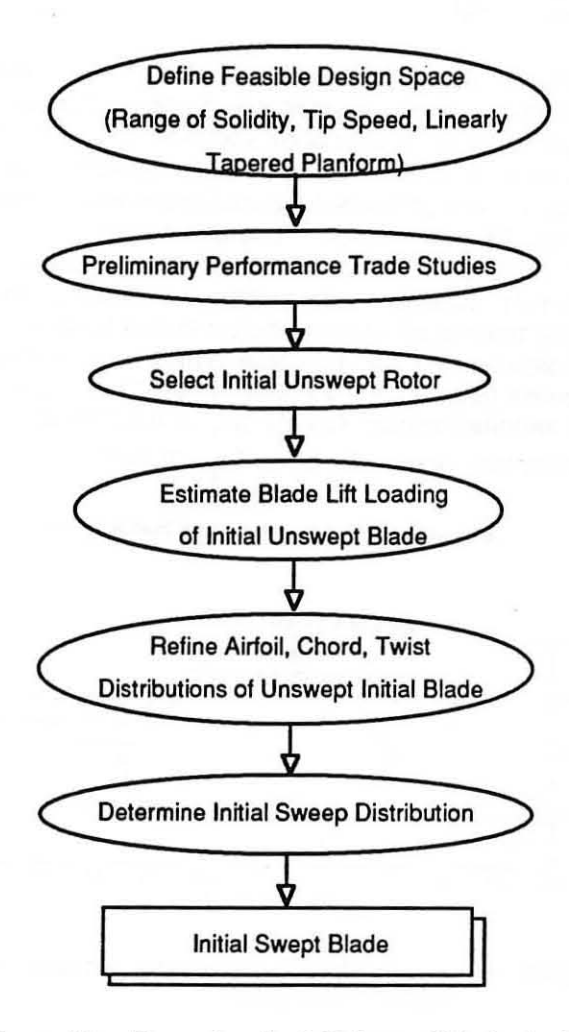


Figure 11 - Procedure for initial swept blade design

o Twist Distribution. For an unswept blade, an "aerodynamic twist" distribution (i.e., the twist of the "zero-lift plane") can be derived from the inflow distribution at the cruise design condition. The "geometric twist" distribution is then obtained by rotating the airfoil sections so that each airfoil's zero-lift plane is aligned with the local inflow velocity:

$$\varepsilon = \alpha_0 + \tan^{-1}\{ (\mu + v_j)/(r/R) \}.$$

The hover-and cruise-optimized twist distributions for the initial baseline planform are shown in Figure 12. The first, most obvious compromise would be to employ the cruise twist distribution in both hover and cruise. Figures 13a and 13b present the Figures of Merit and cruise efficiencies of two rotors with blades that differ only in twist. It can be readily observed that while the rotor with the hover-optimized twist incurs a severe cruise performance penalty at all levels of cruise thrust, both rotors perform equally well in hover at and around the hover design thrust condition. Selecting the cruise-optimized distribution as the candidate twist for the baseline unswept blade is, therefore, a justifiable option.

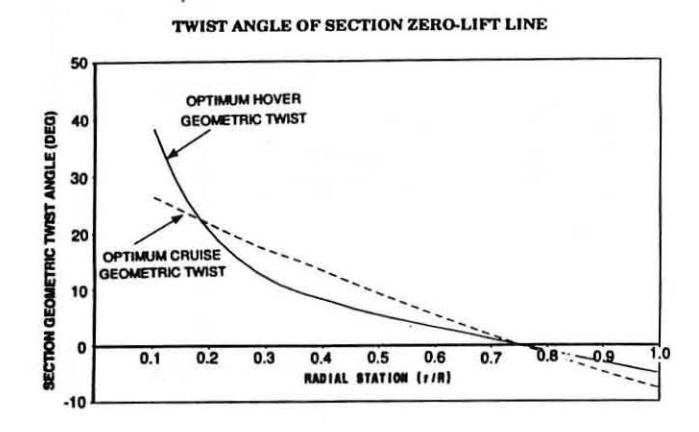
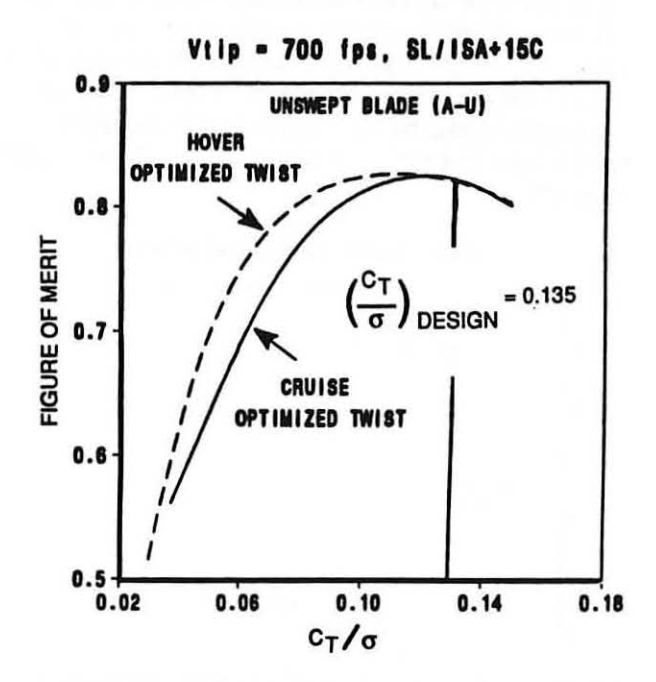


Figure 12 - Optimum twist distributions for hover and cruise

Chord Distribution Compromises - The chord distribution of the baseline unswept blade was refined using the planform determination procedure of Reference 7. This procedure computes the planform of an unswept blade for which the radial distribution of optimum lift coefficient has been prescribed. The Betz condition for minimum induced loss on propellers in axial flight dictates that the wake displacement velocity be radially constant. The displacement velocity of the vortex wake,  $v_0 = v_1/\cos\phi$ , is the speed with which the helical wake travels downstream relative to the surrounding air. The blade loading for minimum induced losses varies radially with vo and can be iteratively solved for to meet a required thrust coefficient. Once the optimum blade loading Cloptc/R has been computed, the spanwise variation in chord, c/R, can be determined from the known Clopt distribution.

For low-speed conditions, C<sub>lopt</sub> may be chosen to be the maximum lift coefficient, C<sub>lmax</sub>; the resulting planform allows maximum lift to be achieved while operating with minimum induced losses. For high speed, there is no "optimum lift" requirement. The loading is low com-

pared to the blade's thrust capabilties, and the blade airfoil sections operate at very low lift coefficient levels. Restricting the sectional lift excursions to low levels,  $C_1 << 0.1$ , would ensure that a section's drag divergence Mach number,  $M_{\rm DD}$ , is as high as possible.



(a) - Hover

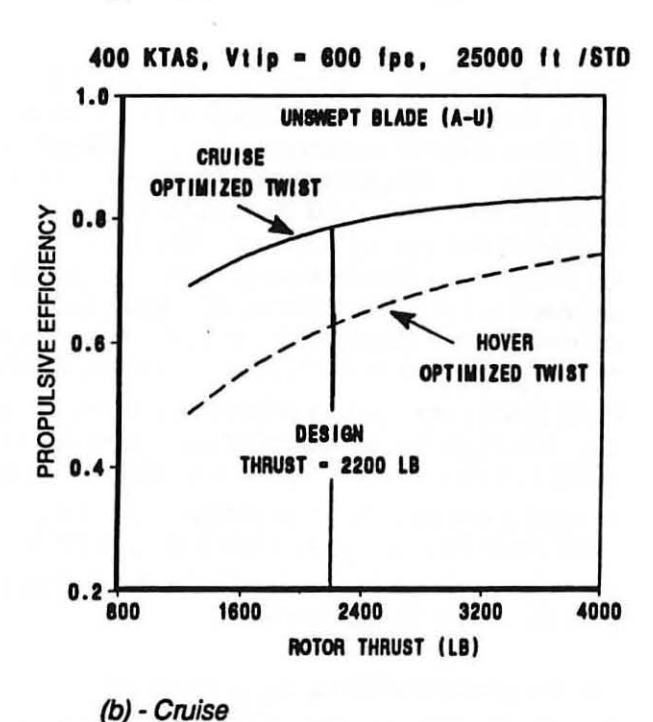


Figure 13 - Hover and cruise performance with hover and cruise optimized twist It was stated earlier that at high-speed cruise conditions the induced power is small, so that blade optimization need not be directed towards the minimization of induced losses. However, since the design has to include good hover performance, for which the induced power losses are significant, some compromises in the planform have to be defined at hover conditions.

During iteration on chord to meet design thrust loading, the lift-to-drag ratio was scaled to account for Reynolds number effects on sectional drag. Tip loss effects were also included, and this caused the planforms to be significantly tapered down in chord near the tip. Flgure 14 shows chord distributions defined for best hover and best cruise performance: an inversely tapered planform is best for cruise, while a highly tapered planform is better suited for hover. It can also be observed that, due to the low disk loading in cruise (cruise T/A = 2.0 lb/ft², hover T/A = 20 lb/ft²), the required cruise solidity ( $\sigma_T$  = 0.1010) is much smaller than needed for hover ( $\sigma_T$  = 0.139).

Solution for Minimum Induced and Profile Power

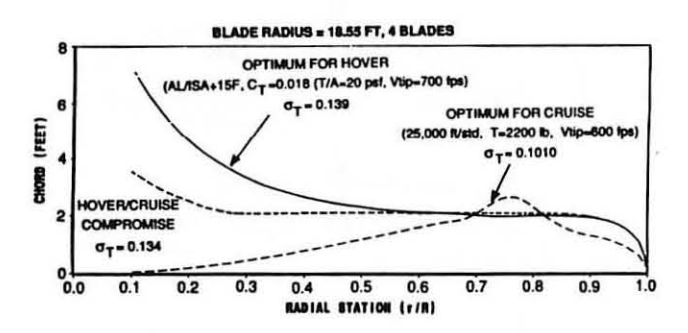


Figure 14 - Chord distribution for optimum hover and cruise performance

The chord distributions required for optimum hover and optimum cruise performance appear to be truly incompatible of each other. In the absence of formal methods of optimization between the hover and cruise requirements, intermediate unswept planforms had to be defined. A "compromise" planform, with the required thrust-weighted solidity of 0.134, is also shown in Figure 14.

<u>Definition of Tip Sweep Schedules</u> - The loading distributions and Mach number environments of baseline unswept blades were compared to the drag divergence Mach number capability of the sections employed. The drag divergence boundary was relieved

by a small Mach number increment (M<sub>DD</sub>+0.01), as explained earlier. Local sweep was introduced so that the normal component of the resultant flow relative to the blade 1/4 chord line would not exceed (M<sub>DD</sub>+0.01). The procedure was incorporated into an inverse solution program to expedite the definition of candidate configurations.

<u>Final Configurations</u> - **Figure 15** summarizes the final swept and unswept planform candidates for 400 knot cruise flight considered in the NASA study. They are identified as blades A, B and C, with qualifiers U or S to indicate whether the tips were unswept or swept. The thrust-weighted solidities of all three blades were maintained at 0.134 in order keep the hover  $C_T/\sigma_T$  at 0.135. On all blades the airfoil distribution has been kept constant, as described in **Table II**, and therefore, all blades have the same twist to meet the 400 knot cruise condition.

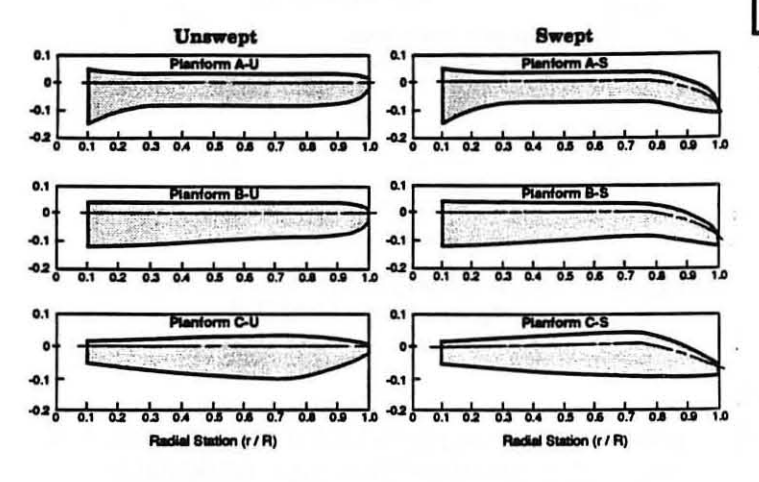


Figure 15 - Candidate blade design planforms

The main characteristics of swept blade configurations A-S and B-S are compared in Figure 16. The swept B-S and unswept B-U blades have the same solidity as the A-blades, but incorporate a linearly tapered planform with 2/3 taper ratio inboard of 0.85R to avoid excessive root chord. The third set of planform variations considered, the "C-blades", have the same airfoil, twist and sweep distributions as the B-blades, but differ in planform. The swept C-S and the unswept C-U blades have an inverse non-linear taper from the root to the 0.75 radial station, and then taper down to 6 inches at the tip. The inverse taper planform was chosen based only upon the cruise-optimum chord distribution given in Figure 15, and has been compromised for hover.

<u>Performance Comparisons</u> - Only key comparisons of blade characteristics will be presented to highlight the main conclusions of the study.

Figure 17 compares the blade loading of unswept A-U and swept A-S blades. It can be observed that sweep effectively redistributes the lift loading, shifting it closer inboard. The effectiveness of sweep in suppressing compressibility drag rise is evident in the radial drag distribution, where it is seen that the profile drag outboard of the swept region is considerably reduced.

Radial Station (r/R)	Airfoil	t/c
0.10	XN-18	0.18
0.20	XN-18	0.18
0.40	VR-12	0.106
0.80	VR-15	0.08
1.0	VR-15	0.08

Note: All airfoil contours interpolated linearly between given blade stations.

Table II - Airfoil distribution over A, B and C blades

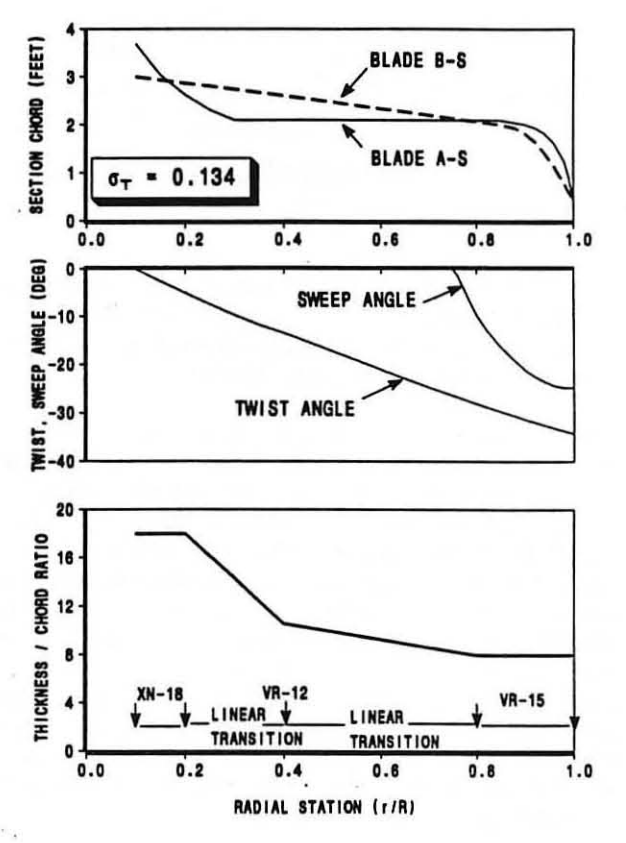


Figure 16 - Definition of A-S and B-S blade characteristics

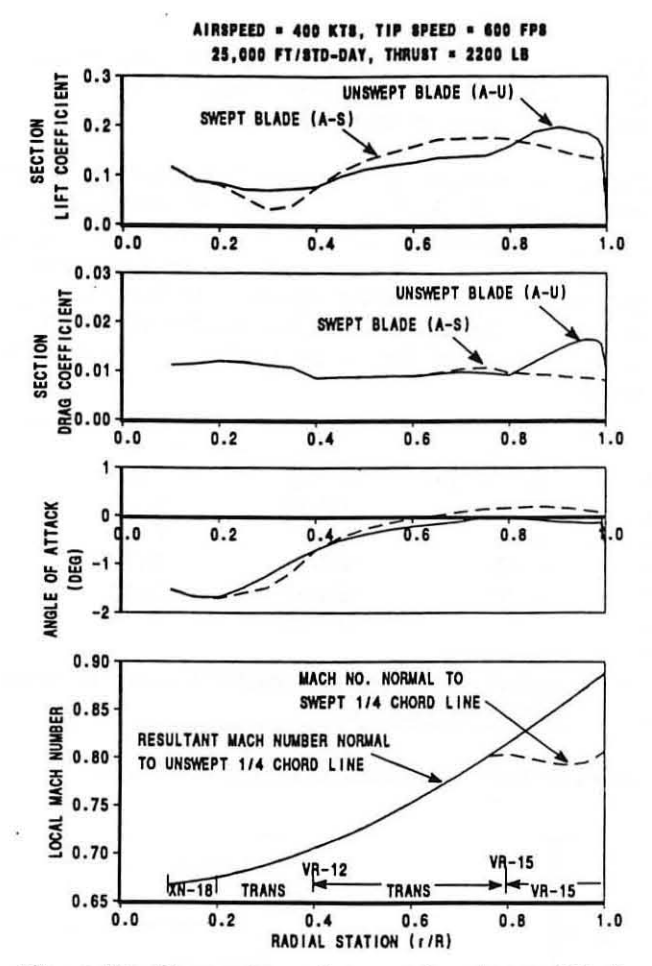


Figure 17 - Comparison of unswept and swept blade loading in cruise.

Figure 18 compares the 400 knot cruise blade loading of swept tip blades A-S and B-S. The distributions of lift and drag loads are nearly identical, indicating that cruise performance should be similar.

Figures 19, (a) and (b), compare the hover and cruise performance of swept A-S, unswept A-U, and swept B-S blades. A-U represents the unswept baseline level of performance. All three rotors have thrust weighted solidity  $\sigma_T = 0.134$ . The swept A-S blade has a 2.6 percent higher cruise efficiency compared to the baseline unswept blade A-U configuration. The swept blade B-S, which is a planform variant of A-S, results in only a 1.6 percent improvement in cruise efficiency relative to blade A-S. The hover performance of the swept blades A-S and B-S are not significantly affected by blade sweep, and the maximum Figure of Merit of the swept and unswept blades remains at the level of A-U.

For swept blades, A-S, B-S, and C-S, hover and cruise performance comparisons are presented in Figures 20, (a) and (b) respectively. Rotor C-S produces the

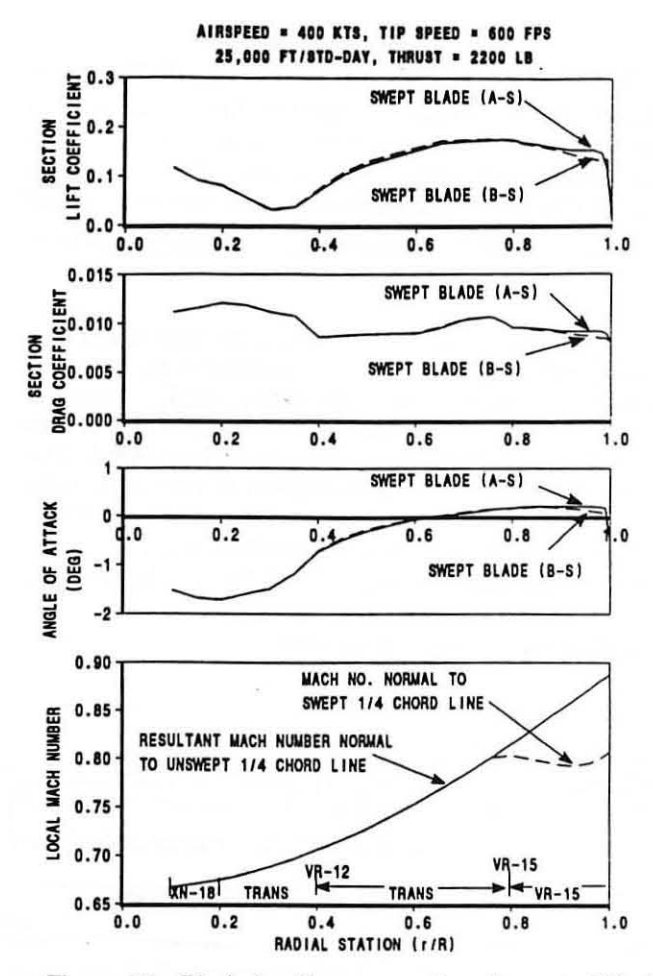


Figure 18 - Blade loading comparison for swept blade configurations A-S and B-S

largest improvement in cruise performance with an efficiency approaching 82 % for the design cruise condition, a 2.5 % improvement over configuration B-S. Blades A-S and B-S yield comparable cruise efficiency improvements, both performing at about 80 percent efficiency at the design cruise thrust. The hover performance of all three swept blades is comparable, with a Figure of Merit exceeding 0.80 at the hover design  $C_T/\sigma_T$ . The hover blade loading of the three blades is illustrated **Figure 21**. It is apparent that, in hover, the inverse taper of blade C-S promotes stall in the root region.

#### THREE-DIMENSIONAL TIP FLOW ENVIRONMENT

The TECH-01 and CAMRAD/JA rotor analysis codes are called "comprehensive" because they combine on a practical level aerodynamics, dynamics and rotor trim procedures which allow the user to model in one computation rotor blade airloads, motions and elastic deflections.

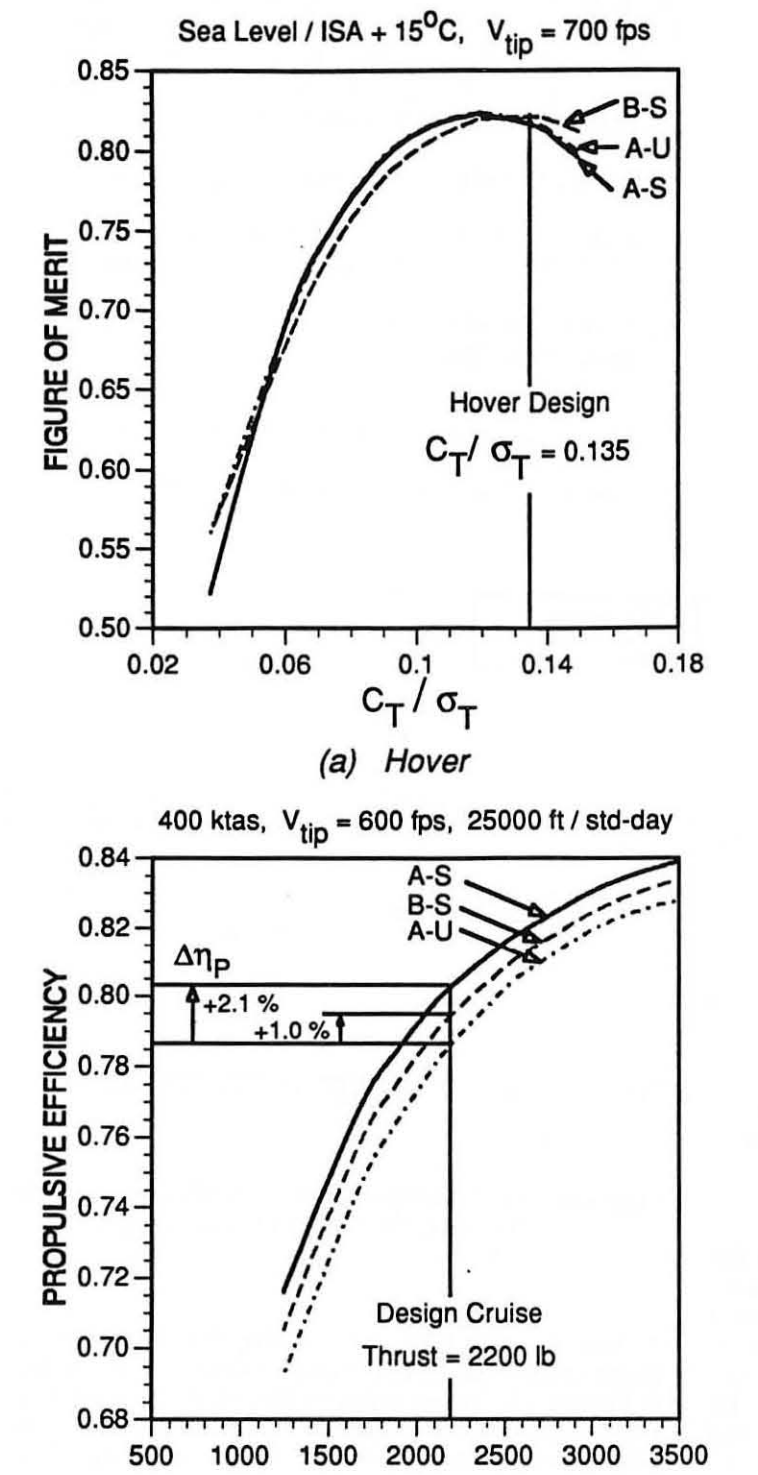
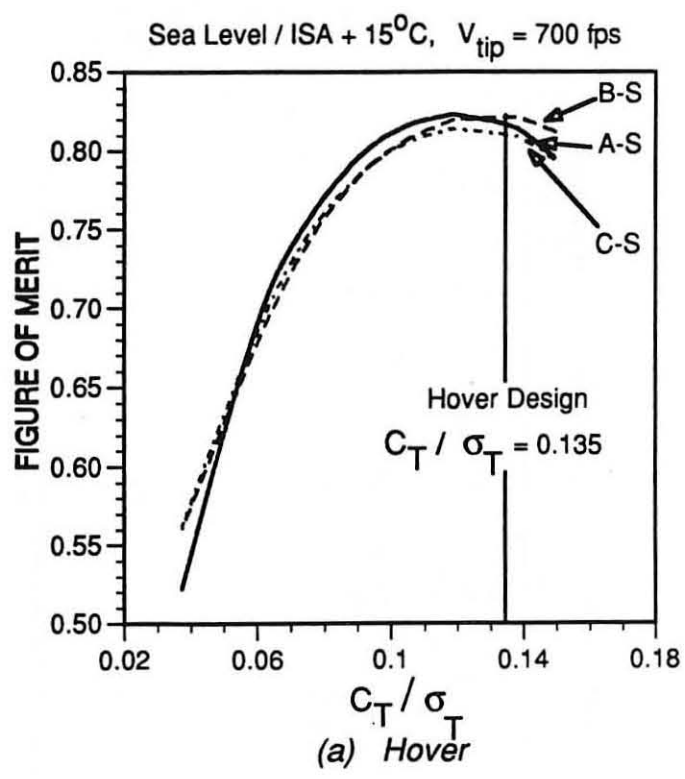


Figure 19 - Comparison of hover & cruise performance of rotor configurations A-U, A-S, and B-S.

ROTOR THRUST (LB)

(b) Cruise



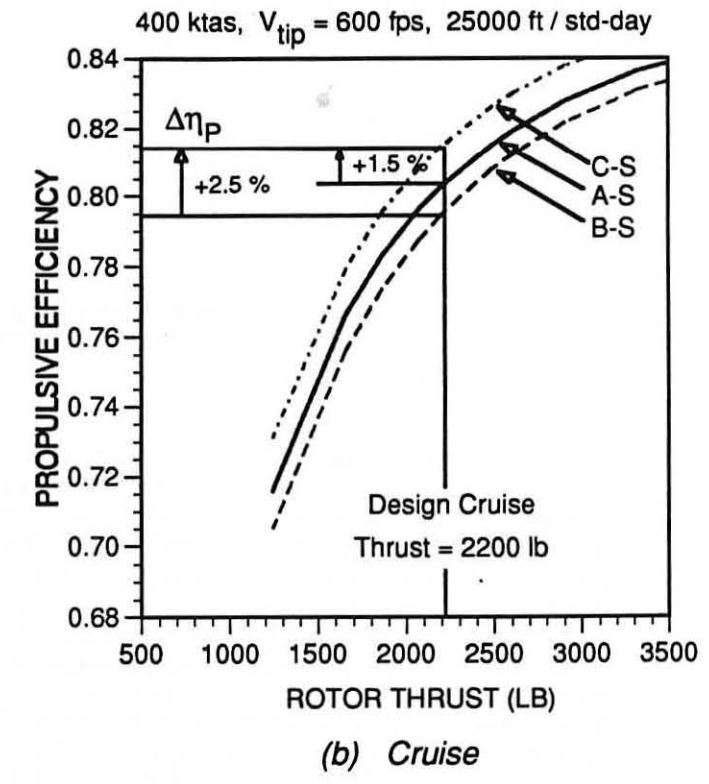


Figure 20 - Comparison of hover & cruise performance of swept rotor configurations A-S, B-S, and C-S.

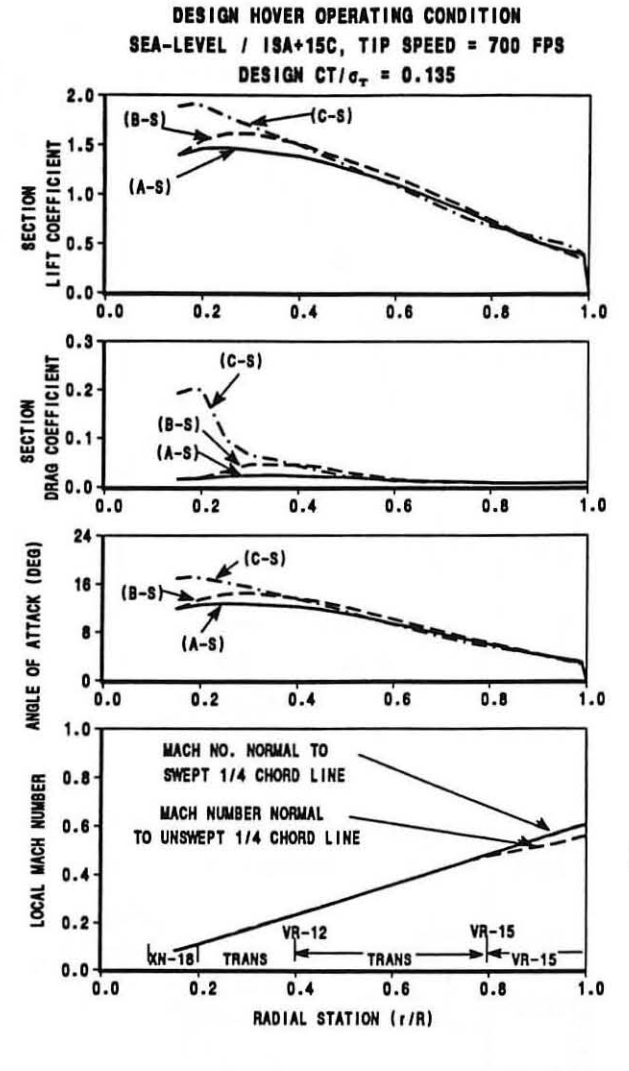


Figure 21 - Comparison of swept blade lift and drag loading in hover, for blade configurations A-S. B-S and C-S

Aerodynamically, the comprehensive codes model the rotor blades by lifting line theory, replacing the threedimensional blade with computation points distributed along a single line. The lifting line models are not adequate near the tip of blades. Two main tip relief models have been introduced in TECH-01. The first, by LeNard<sup>4</sup>, corrects the profile drag. The second model is an empirical approximation of local changes in the sectional lift-curve slope close to the tip of rotor blades. It was formulated for use with lifting line theory, and it is currently used only at transonic conditions (approximately for M > 0.6). This lift-curve slope correction was derived from blade pressure measurements in hover by Caradonna and Tung<sup>17</sup>, and is referred to as the Levacic correction. Details are described in Reference 3.

In the absence of adequate test evidence, trends on the effect of airfoil and blade planform variation at transonic tip Mach numbers have been obtained by means of rotor CFD codes, specifically the FPR<sup>13,14</sup> code, and a preliminary axial-flow modification of FPR.

FPR and an axial modification of FPR were used to:

- Evaluate 3-D lift curve slope trends, for use in TECH-01 through the Levacic approximations, and
- Assess airload differences between straight and swept blade tips.

Configuration: Rectangular tip helicopter blade Analysis: FPR edgewise flight, 90 deg. azimuth, M.,...=0.85

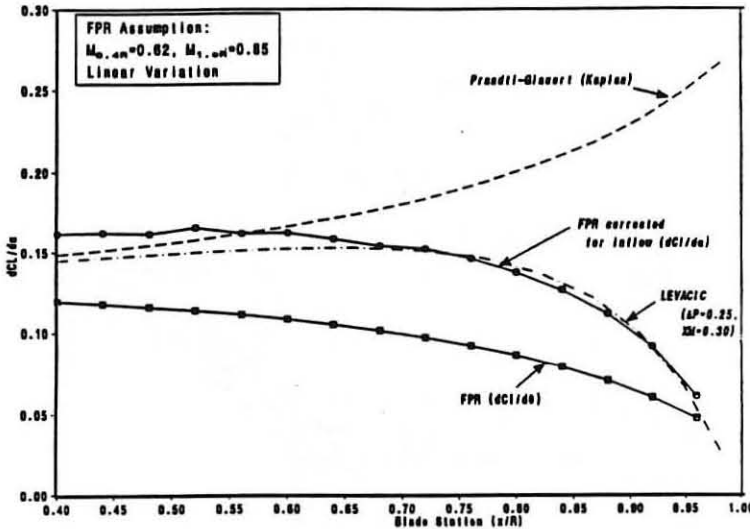


Figure 22 - FPR estimate of the local lift curve slope for a rectangular blade planform in edgewise flow

A way of using FPR in evaluating 3-D tip effects in terms of the local lift curve slope changes is illustrated in FIgure 22. In the example shown, the blade had a rectangular planform and a thin tip airfoil (6% section) held constant from the 0.75R station to the tip. The FPR solution was in the helicopter mode, for an untwisted blade, with symmetrical airfoils at the  $\Psi = 90^{\circ}$  position. Two pitch angles were evaluated: e.g.,  $0^{\circ}$  and 0.5°, with tip speed and advance ratio set for a given tip Mach number. At the  $0^{\circ}$  pitch level FPR would verify that the model produces zero lift. The lifting solution provided local blade pitch sensitivities,  $(dC/d\theta)$ , which were corrected to actual lift curve slope

values (dC/dα) by approximating induced velocity corrections from a simple trailed wake model. Also shown in Figure 23 is a line with a fit of FPR results by the Levacic equations, and a two-dimensional lift curve slope trend. Away from the tip, the lift curve slope from FPR exceeds the Prandtl-Glauert trend, but there is evidence such overprediction is typical of all current CFD codes, and it does not detract from the usefulness of the results.

Configuration: Straight VR-15 tiltrotor blade Analysis: FPR(Axial) & TECH-01 (results adjusted) V<sub>axial</sub>=300 kts., 0=57. degrees, M<sub>1/p. hol</sub>.=0.77

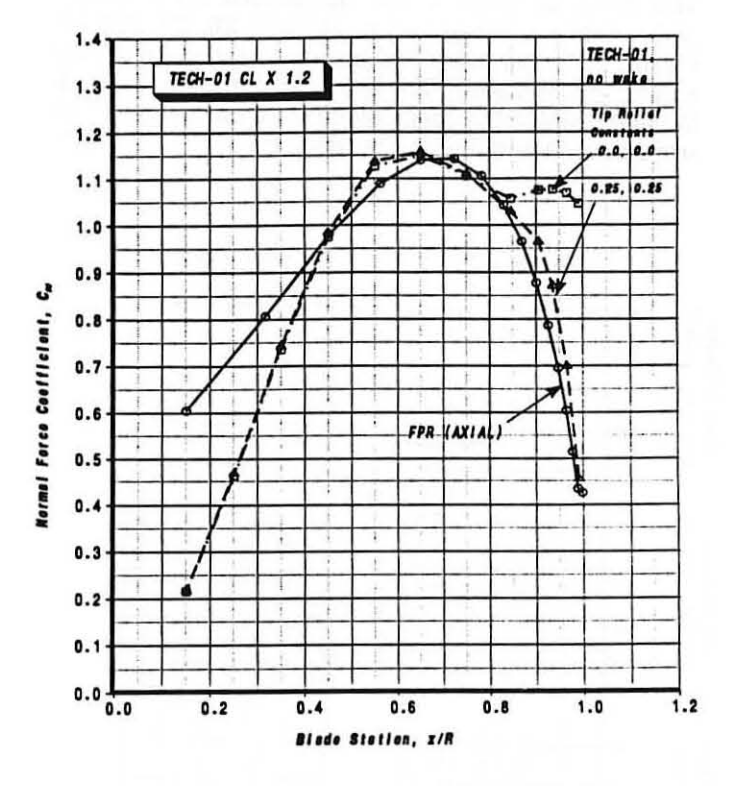


Figure 23- Comparison of Axial-FPR and TECH-01 lift distributions for an untapered tiltrotor blade planform in axial flight at 300 knots.

Figure 23 compares FPR and TECH-01 results from axial flight calculations carried out with a rectangular blade planform and airfoils representative of high speed tiltrotor blades. The twist was set to provide zero lift along the blade at a reference pitch angle (i.e., the zero-lift plane of the blade was lined up with the local inflow angle, φ). The TECH-01 normal force coefficient distribution includes the Levacic correction and is close to the FPR results; however, the TECH-01 values were scaled by a factor of 1.2 to account for the overprediction by CFD methods described earlier.

This overprediction is not critical in the assessment of the Levacic correction (which models the ratio of 2-D to 3-D lift curve slope values as a function of blade geometry and flight conditions) but it poses some questions about the validity of calculations coupling rotor CFD and comprehensive rotor analysis codes. For the purposes of the present study, the Levacic approximation was considered adequate for both straight and swept tip blades.

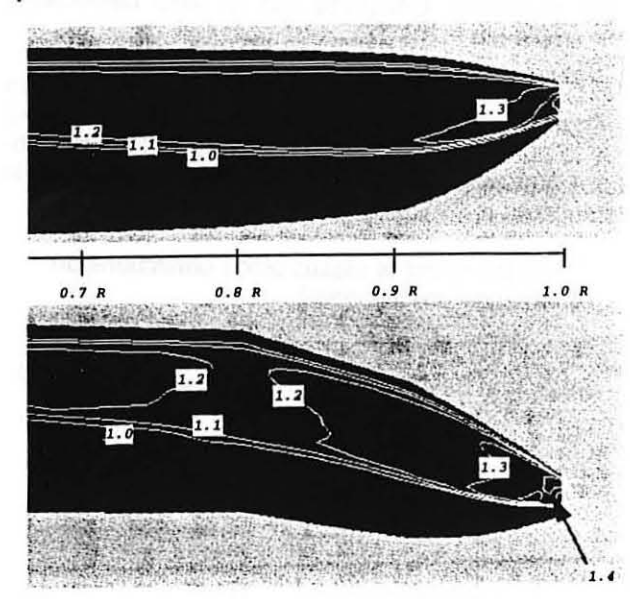


Figure 24 - Comparison of Axial-FPR Mach number contours for straight B-U and swept B-S planforms in 400 knot flight. Upper surfaces.

Figure 24 compares constant Mach number contours over the upper surfaces of straight configuration B-U and swept configuration B-S in 400 knot axial flight. Only the outer 30% of span is shown. The flow solutions were obtained by means of axial-FPR, with significant help from Army AFDD personnel. The FPR results for the two planforms appear to be qualitatively correct, and have yielded tip relief trends which were incorporated in the Levacic correction. examination shows that the swept tip did not appear to benefit of any of the Mach number relief expected from tip sweep, although no de-localization was observed for either tip. This may be due to the fact that, since the FPR calculations were to provide only tip relief trends, no attempt was made to match more exact trim conditions. It is also possible that the twist of the swept configuration could be further optimized, and there is experimental and analytical evidence showing that simple superposition methods fail in properly combining tip chord taper and tip sweep aerodynamic trends<sup>18,19</sup>. A better understanding of tip sweep effects will require the review of more test evidence, and more systematic CFD calculations, tasks well beyond the scope of the NASA study<sup>3</sup>.

# AXIAL-FLOW ANALYSIS OF SELECTED CONFIGURATIONS (TECH-01)

While the B-08 analysis, used to define the final configurations of Figure 16, did not employ the 3-D lift-curve slope corrections described in the previous section, it did, however, use the Prandtl tip loss factor, which is conditionally satisfactory for most preliminary design purposes. Complete 3-D tip relief corrections were employed in the TECH-01 calculations.

TECH-01 calculations for the swept tip, B-S planform configuration and its unswept counterpart, B-U, were used to pursue the investigation of a few key proprotor design issues. Two questions will be addressed in this section:

- 1) What is the effect of elastic blade deflections on performance and airloads?
- 2) How will the straight and swept blades perform below and beyond the 400 knot design condition?

Some assumptions were necessary before introducing elastic effects into the TECH-01 calculations. First, it was assumed that the blades are rigidly attached to the hub, as in conventional propellers. This was done while recognizing that a gimbaled hub arrangement would have to be used in an actual design. The second assumption had to do with blade structural properties.

The structural properties used in the present investigation were scaled from known tiltrotor configurations and from available preliminary design information. They only represent a starting point. The assumed structural characteristics of the straight (B-U) and swept (B-S) blade tips are summarized in Figures 25a, b.

The effect of blade elastic deflections on proprotor performance is illustrated in Figures 26, 27 and 28. Figure 26 summarizes the proprotor thrust levels assumed for the various flight speeds, at the 25,000 ft altitude for which the calculations were carried out. Figure 27 compares the performance of the straight and

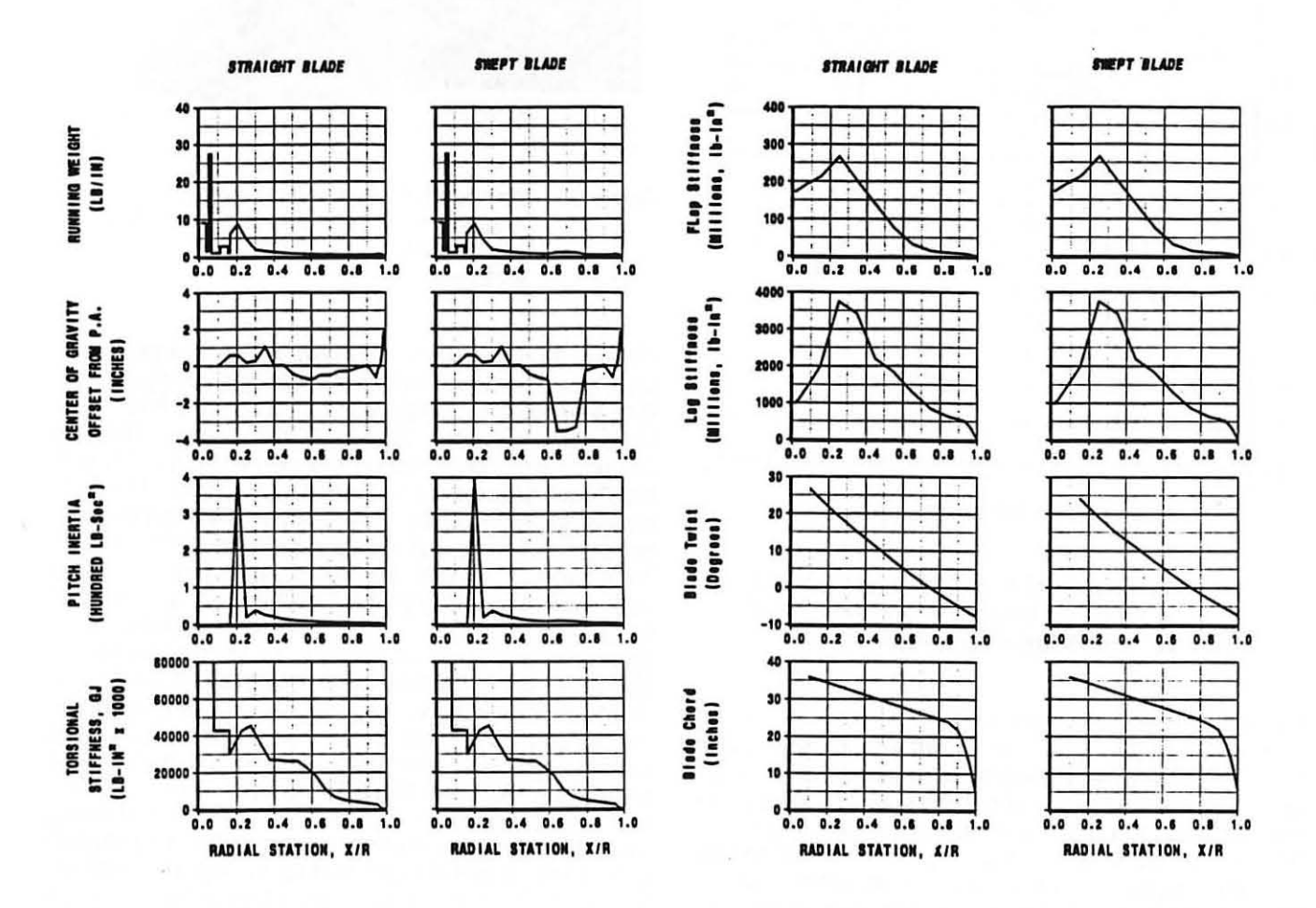


Figure 25 a - Blade properties for straight and swept blades (continued)

Figure 25 b - Blade properties for straight and swept blades (concluded)

swept blades, both rigid and elastically deformable, in terms of proprotor efficiency. The effect of elastic deflections on performance was shown to be generally negligible, for the structural properties employed in this study. Elastic effects appear to penalize the performance of the swept tip blades at flight speeds beyond 400 knots, but, overall, the performance of the swept blades is always above the level of the straight blades. Figure 28 also shows that at 370 knots the unswept blades have the same efficiency as the swept tip blades at 400 knots. Reducing the thickness of the tip airfoil from 8% to 7% would increase its drag divergence Mach number by approximately  $\Delta M_{DD} = 0.01$ , and could, potentially, improve the cruise speed of the unswept tip blades to nearly 380 knots.

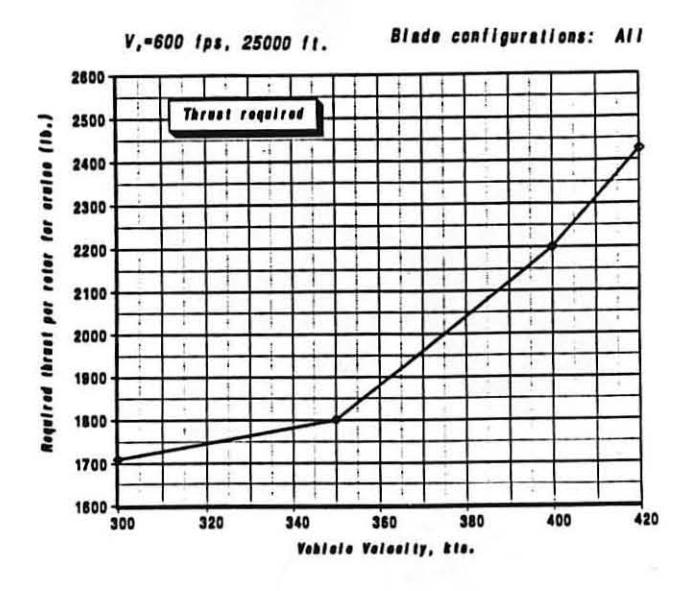


Figure 26 - Required proprotor thrust levels for flight speeds between 300 knots and 420 knots at 25,000 ft altitude

Figure 28 summarizes the steady elastic twist deflections experienced by the straight and swept tip blades between 300 and 420 knots. Again, these results should be considered preliminary. The swept tip blades experience larger elastic twist deflections than the straight blades because of the lift contribution of the swept portion of the planform to the total blade torsional moment. On swept tip configuration B-S, the steady\_elastic twist change varies from 0.85° at 300 knots to 1.07° at 400 knots. The straight blades, B-U, experience negligible steady twist deflections at 300 knots and 0.5° at 400 knots. Beyond 400 knots the elastic twist can be expected to grow rapidly with increasing flight speed, and, as compressibility effects become significant, the torsional deflection of the straight blades may even exceed the deflection on the swept blades (as observed on helicopter rotors). It should be noted, however, that in TECH-01 the tip airloading and the aerodynamic moments are almost totally dependent on 3-D empirical corrections. These corrections are approximately known for the 400 knot condition, but have not been verified for speeds beyond 400 knots.

> Biado configurations: B-U, B-S Analysis: TECH-01 V,=600 fps, 25000 ft.

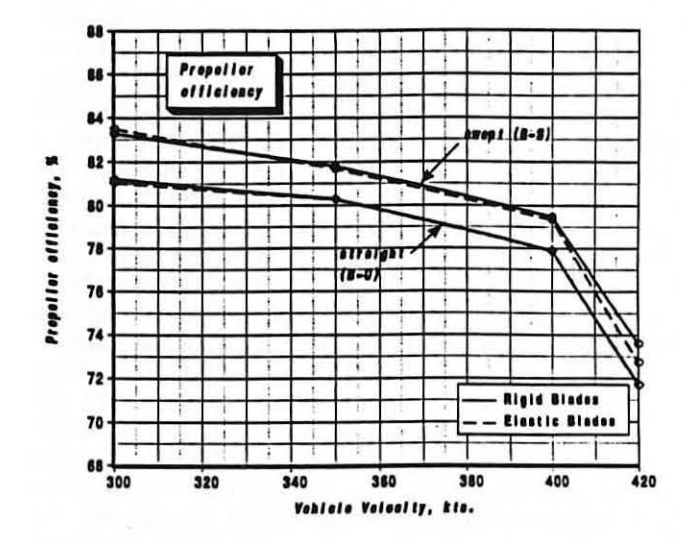


Figure 27 - Effect of elastic deflections on proprotor efficiency at flight speeds between 300 and 420 knots

Blade configurations: B-U, B-S Analysis: TECH-01 V,=600 fps, 25000 ft.

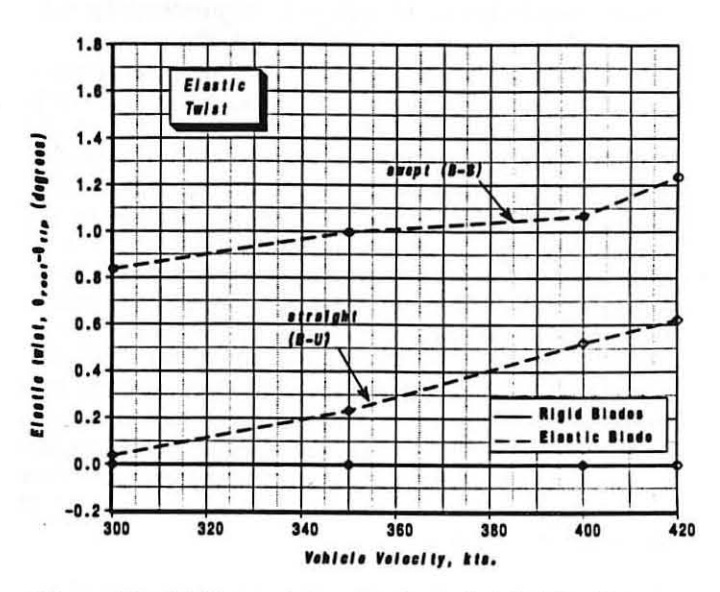


Figure 28 - Estimated steady elastic twist deflections for straight and swept blades at flight speeds between 300 and 420 knots

#### INTERACTIONAL AERODYNAMIC EFFECTS

In purely axial flight there are no azimuthal variations in blade airloads and flow field properties, and no in-plane loads are produced. However, when the flow is perturbed by interference velocities or by changes in pitch and yaw, azimuthally varying blade airloads and net in-plane hub forces are generated.

The effect of wing and fuselage interference velocities on rotor performance and vibratory airloads was estimated by means of VSAERO<sup>12</sup> flow field velocities introduced into the TECH-0110,11 rotor analysis. Without interference velocities, TECH-01 models isolated rotors, namely rotors meeting a uniform free-stream velocity distribution. The isolated rotor in uniform flow does not display any vibratory forces, other than negligible fluctuations due to gravity (since in the airplane mode the disc plane is perpendicular to the earth's surface during level flight). Large vibratory airloads, however, may be experienced in the presence of wing and body flow interference. The magnitude of the interference effects is a function of wing loading and can be expected to be more significant at high incidence angles. The effect of flow interference on performance and airloads was investigated for both structurally rigid blades and elastic blades. Limited flow interference calculations were also carried out to assess hub effects. As predictable, it was found that allowing blade motions in the flapping and lead-lag directions significantly reduces hub forces and moments. Hub design issues will have to be addressed in future studies. Most of the calculations in Reference 3 were intended to quantify the magnitude of the flow effects involved. and were carried out assuming hingeless hubs.

While actual wing and fuselage configurations for high speed tiltrotors remain to be defined, the most significant interference effects can be meaningfully investigated by assuming a generic wing-body geometry. The preliminary wing/body combination used in the present study, illustrated in Figure 29, has moderately swept-forward wings placed on top of a streamlined fuselage. Tail surfaces were not modeled as not relevant to the rotor interference problem. Figure 30 also shows the placement of the rotor disc planes relative to the wings and summarizes the sign conventions of the quantities involved. The VSAERO calculations were carried out for the wings set at the incidence necessary for operation at typical flight speeds and gross weights, assuming that the rotors can always be oriented so that the disc plane is exactly perpendicular to the direction of flight. This assumption simplifies the assessment of the effect of interference velocities at the rotor disc plane.

Figure 30 shows isometric displays of the radial and azimuthal variations in normal and tangential interference velocities for a 400 knot flight condition. The

largest fluctuations in interference velocities take place in the vicinity of the wing's leading edge ("wing upwash"). The proprotor wake also induces pressure fluctuations on the wing and on the tail surfaces, but an assessment of these sources of vibration was outside of the scope of the present study.

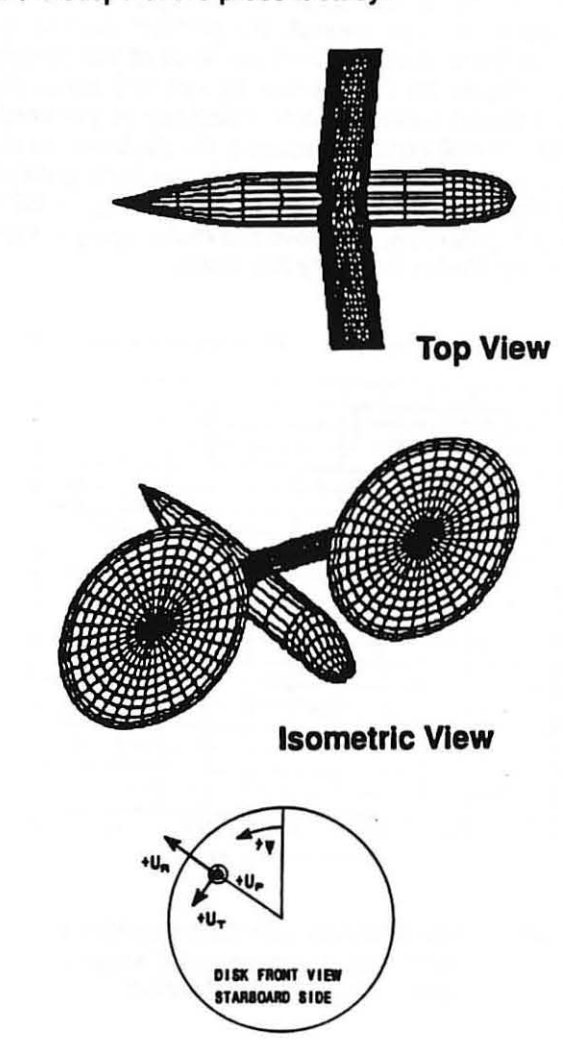
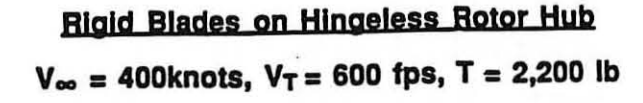


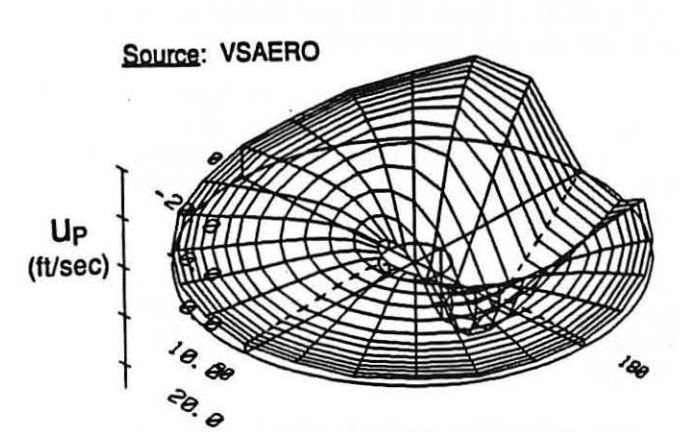
Figure 29 - Placement of the rotor and disc planes in the VSAERO panel model

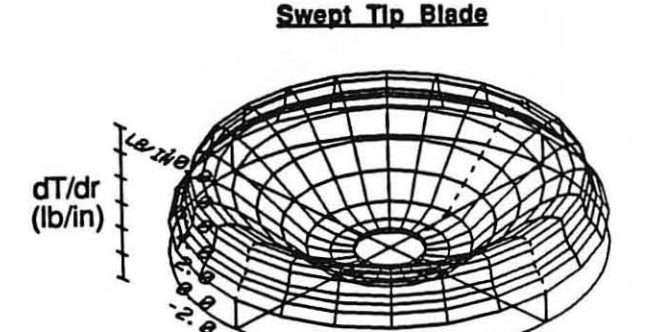
TECH-01 calculations were carried out at 300 and 400 knot flight speeds for structurally rigid and elastically deformable blades, for both straight and swept tip configurations. Hingeless and articulated hubs were examined. In all cases, the calculations first addressed the isolated rotor conditions and then were repeated with the interference velocities as described in Figure 30. Figure 31 compares the radial and azimuthal variation in thrust loading for swept tip blades, without and with interference velocities, at a 400 knot flight condition. The blades were rigid and were attached to a rigid hub. Being rigid, no significant differences in interference effects were observed between the

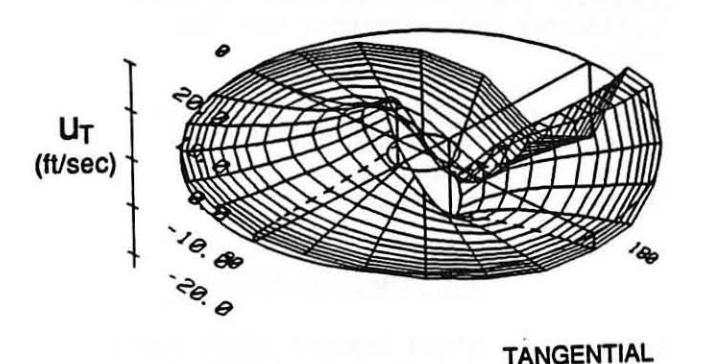
# Interference Velocities at 400 knots. $\alpha = -2.3^{\circ}$ , 25,000 ft



THRUST LOADING (lb/in)







NORMAL

Uniform Flow

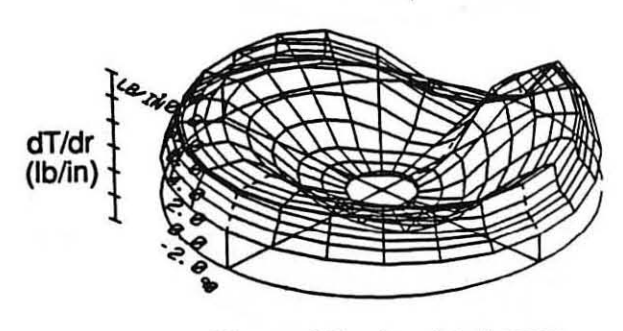


Figure 30 - Radial and azimuthal variation of wing and fuselage interference velocities at the rotor disc plane, at 400 knots

Wing and Fuselage Interference

straight and swept tip blades. Subsequent calculations involving elastically deformable blades only showed a higher harmonic content in the blade loading, while the magnitude of the vibratory airloads did not appreciably change from the rigid blade baseline. The validity of the calculations involving elastic deflections is a function of the assumed structural properties, something that needs to be addressed in future studies. Quite predictably, the introduction of blade flapping had the effect of reducing the magnitude of the vibratory airloads, confirming the importance of hub definition early in the design cycle.

Figure 31 - VSAERO and TECH-01 estimated effect of wing-fuselage interference on blade thrust loading time history at 400 knots.

Non-Axial Flow Conditions - Vibratory airloads of the magnitude shown in Figure 32 would probably be unacceptable, and they are due to just interference velocities. Figure 32 shows the effect of 1° and 2° deviations from pure axial flow conditions at 400 knots, without interference velocities. The compounded ef-

fect of non-axial flow and wing-fuselage interference was not addressed at this time, but it can be expected to be even more significant in terms of the vibratory airloads produced. For the future, however, we expect that high vibratory airloads can and will be relieved by advanced hub and blade designs. All the elements of the necessary methodologies are already at hand, but they certainly need to be validated. Although only exploratory in nature, these calculations underscored the importance of comprehensive predictive methods to support the design of advanced proprotor blades. They also underscored the need for detailed test evidence to validate all aspects of the analytical models involved.

#### Elastic Blades on Hingeless Rotor Hub

 $V_{\infty} = 400$  knots,  $V_{T} = 600$  fps, T = 2,200 lb

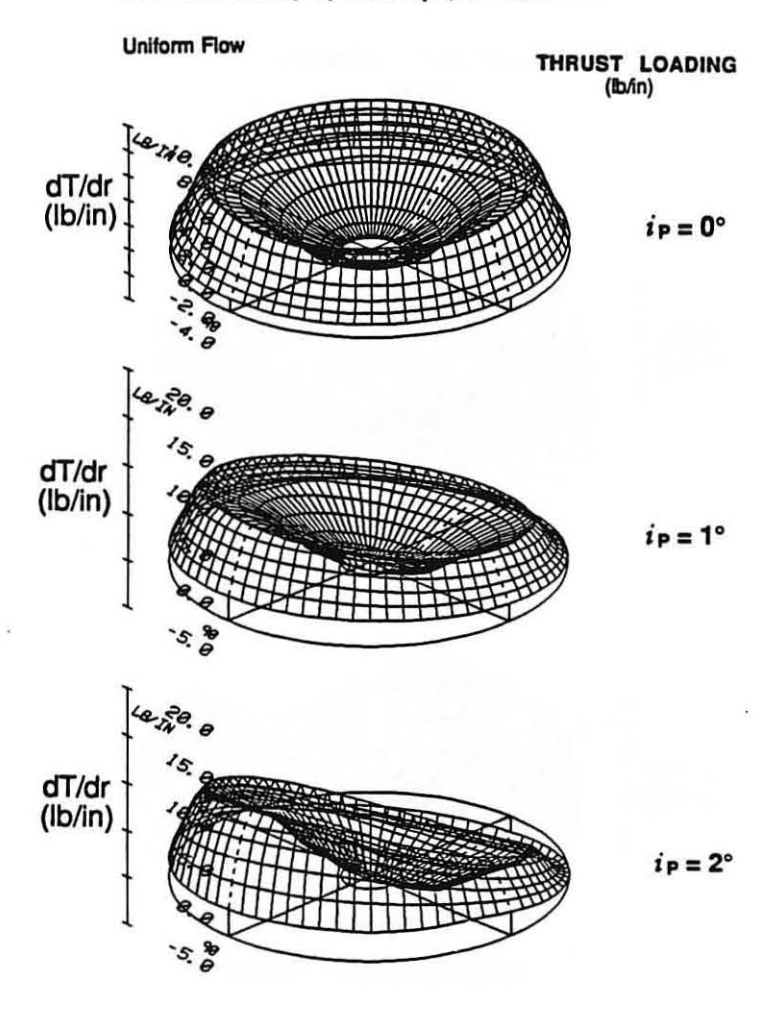


Figure 32 - TECH-01 prediction of the effect of proprotor incidence angle on the radial and azimuthal variation in thrust loading at 400 knots

#### CONCLUSIONS

- o The conventional helicopter rotor wisdom of designing for minimum induced power with the airfoil sections operating near maximum L/D does not apply in high speed tiltrotor blade design.
- o Aerodynamically efficient blade planforms with tip chord taper and sweep over no more than 30% of the blade span are feasible for flight speeds up to 400 knots.
- o For flight speeds below 380 knots it should be possible to adequately reduce compressibility effects without tip sweep by reducing tip airfoil thickness.

- o The performance of high speed tiltrotor blades may be as significantly influenced by root-end thickness as it is by tip phenomena. High speed tiltrotor blade structural requirements will have to be defined in better detail before the impact of root end thickness effects, and possible root-end sweep, can be quantified.
- o The estimated elastic blade deflections during high speed flight were small, and were achieved without unusually demanding blade stiffness requirements. Manufacturing tolerances and blade-to-blade discrepancies remain a concern.
- o Aerodynamic interference and non-axial flow conditions are a potential source of large vibratory airloads. These effects will have to be addressed by hub design.
- o The rotor CFD methods employed in the present study yielded useful trends, but grid modeling difficulties precluded more extensive computations. User-friendly grid generations methods are a high priority.
- o Better empirical models for tip relief effects are needed for practical design studies. CFD can be expected to provide useful trends, but these will have to be validated experimentally.

#### RECOMMENDATIONS

- o Investigate thinner inboard airfoils and inboard forward sweep to help to meet blade structural requirements without penalizing aerodynamic performance.
- o Examine the feasibility of reducing tip sweep requirements through the use of thinner tip airfoils.
- o In the present investigation the design variables were examined one at a time, independently of each other. Future, more rigorous, optimization will have to address combinations of twist, chord and airfoil changes.
- o Quantify proprotor performance improvements possible by local twist variations. Include elastic twist considerations in the blade design criteria.
- Carry out systematic calculations by means of rotor CFD methods (e.g., FPR), to define an improved empirical model of 3-D tip relief suitable for high speed proprotor applications.
- o Hub design will have to be introduced early in the overall design cycle. The impact of improved hub designs remains to be investigated.

- o More systematic calculations will have to be carried out to quantify the effect of combined non-axial flow conditions and wing / body interference effects. While current methods can model interference effects, test data are needed for validation.
- o At the earliest possible opportunity a proprotor model should be built and a wind tunnel test conducted to provide quantitative evidence for the most critical performance, blade load, noise and vibration issues.

#### REFERENCES

- Thompson, P., et al., "Civil Tiltrotor Missions and Applications, Phase II: The Commercial Passenger Market Final Summary Report", NASA CR-177576, February 1991.
- Wilkerson, J. B., Schneider, J. J. and Bartie, K. M.: "Technology Needs for High-Speed Rotorcraft", NASA CR-177585, May 1991.
- 3. Dadone, L., Derham, R., Liu, J., Wilkerson, J., Yablonski, M. and Ziegenbein, P.: "Detailed Rotor Design trade Study", to be released as a NASA CR report in 1994.
- LeNard, F. and Boehler, G.D.: "Inclusion of Tip Relief in the Prediction of Compressibility Effects on Helicopter Rotor Performance", USAAMRDL TR-73-71, December 1973.
- Liu, J., Paisley, D.J. and Hirsh J.: "Tiltrotor Aerodynamic Blade Design by Numerical Optimization Method", presented at the 46th Annual Forum of the American Helicopter Society, Washington, D.C., May 1990.
- Paisley, D.J.: "Rotor Aerodynamic Optimization for High-Speed Tiltrotors", presented at the 43rd Annual Forum of the American Helicopter Society, St. Louis, MO, May 1987.
- 7. Liu, J. and McVeigh M.A.: "Design of Swept Blade Rotors for High-Speed Tiltrotor Applications", presented at the AIAA Aircraft Systems Design Conference, Baltimore, MD, September 23-25, 1991.
- 8. Himmelskamp, H.: "Profiluntersuchungen an einem umlaufender Propeller. Diss. Gottingen 1945", Mitteilungen ans dem Max-Planck-Institut fur Strömungsforschung, Gottingen, No. 2 (1950).
- Johnson, W.R.: "CAMRAD-JA. A Comprehensive Analytical Model of Rotorcraft Aerodynamics and Dynamics", Volume 1, Theory Manual, Johnson Aeronautics, 1988.

- Dadone, L.: "Description of Input Data for the B-65 Forward Flight Rotor Performance and Airloads Analysis", Boeing Document D210-12649-1, August 1987.
- 11. Tarzanin, F. and Ranieri, J.: "Aeroelastic Rotor Analysis Program C-60", Boeing Report D210-10371, revised 1978.
- Maskew, B.: "Program VSAERO. A Computer Program for Calculating the Nonlinear Aerodynamic Characteristics of Arbitrary Configurations", NASA CR-166476, November 1982.
- 13. Strawn, R.C. and Caradonna, F.X.: "Conservative Full Potential Model for Unsteady Transonic Rotor Flows", AIAA Journal, Volume 25, No. 2, pp. 193-198, February 1987.
- 14. Bridgeman, J.O., Strawn, R.C., Caradonna, F.X. and Chen, C. S.: "Advanced Rotor Computations with a Corrected Potential Method", presented at the 45th Annual Forum of the American Helicopter Society, Boston, MA, May 1989.
- 15. McVeigh, M.A. and McHugh, F.J.: "Aerodynamic Design of the XV-15 Advanced Composite Tilt Rotor Blade", presented at the 43rd Annual Forum of the American Helicopter Society, St. Louis, MO, May 1983.
- 16. Rosenstein, H. and Clark, R.: "Aerodynamic Development of the V-22 Tilt Rotor", paper AIAA-86-2678, presented at the AIAA/AHS/ASEE Aircraft Systems, Design & Technology Meeting, Dayton, OH, October 1986.
- 17. Caradonna, F., and Tung, C.: "Experimental and Analytical Studies of a Model Helicopter Rotor in Hover", NASA TM-81232, September 1981.
- 18. Lorber, P.F.: "Aerodynamic Results of a Pressure-Instrumented Model Rotor Test at the DNW", presented at the 46th Annual Forum of the American Helicopter Society, Washington, D.C., May 1990.
- 19. Shanley, J.P., Moffitt, R.C. and Davis, S.J.: "Systematic Correlation of the EHPIC Hover Analysis", presented at the 46th Annual Forum of the American Helicopter Society, Washington, D.C., May 1990.